

Validity of perturbation theory in calculations of magnetocrystalline anisotropy in Co-based layered systems

M. Cinal*

Institute of Physical Chemistry, Polish Academy of Sciences, 01-224 Warsaw, Poland

(Dated: July 14, 2025)

Validity of second-order perturbation theory (PT) is examined for magnetocrystalline anisotropy (MCA) energy in Co films with enhanced spin-orbit coupling (SOC) and Co/Pt bilayers. Comparison with accurate results obtained with the force theorem (FT) reveals significant discrepancies in the dependence of the MCA energy on the Co thickness. For systems with strong SOC, the PT fails to correctly describe the oscillations of the MCA energy, largely overestimating their amplitude and even failing (for Co/Pt bilayers) to reproduce their specific periodicity. These failures specifically concern the dominating oscillations with the 2-monolayer period which arise from pairs of quantum well (QW) minority-spin d states in the Co layer, degenerate at the centre of the Brillouin zone (BZ). A simplified model of such states demonstrates that the large discrepancies between PT and FT predictions arise from the breakdown of the PT in a region around the BZ centre where the energy spacing between states within each pair is small compared to the SOC strength. It is also shown that the oscillation amplitude of the MCA energy calculated with the FT is limited by the finite energy spacing between consecutive QW pairs, whereas this amplitude grows quadratically with the SOC strength in the PT calculations. Furthermore, for weak and moderate SOC strengths, the accuracy of the PT diminishes with increasing the ratio of the SOC constant to temperature which defines the broadening of energy levels. This explains why the PT overestimates the amplitude of MCA energy oscillations at low temperatures, even for the Co film with a relatively weak nominal SOC. For the Co/Pt bilayer, the strong temperature dependence of the oscillation amplitude in the PT approach leads to the MCA energies which are markedly different at low and zero temperatures, of opposite sign and several times larger in magnitude, compared to the FT results.

Keywords: magnetocrystalline anisotropy, spin-orbit coupling, force theorem, perturbation theory

I. INTRODUCTION

Magnetic anisotropy is one of the key properties that determine the magnetic structure and affect the dynamics of magnetic materials. It describes the dependence of the system energy on the magnetization direction, with the energy minimum corresponding to preferred magnetization orientation, the easy axis. Two main sources contribute to magnetic anisotropy: the dipole-dipole interaction, which results in the shape anisotropy dependent on the sample geometry, and the spin-orbit coupling (SOC), which modifies the system's electronic structure in a manner dependent on the magnetization direction, leading to the magnetocrystalline anisotropy (MCA) [1–5]. MCA is enhanced in ferromagnet/nonmagnet (FM/NM) layered systems due to the reduced symmetry at interfaces and the SOC of NM. In films with high-symmetry surfaces, the easy axis is oriented either in-plane or out-of-plane, while a tilted orientation of the easy axis is observed for films with stepped surfaces [6, 7]. Among layered systems, FM/heavy metal (FM/HM) bilayers are of particular interest. In these bilayers, an in-plane electric current in a layer of metal with strong SOC, such as Pt or Ta, generates transverse spin current that flows into the FM layer enabling magnetization switching [8–10], while the lack of the inversion symmetry is essential for emergence of a finite spin-orbit torque acting on the magnetization. In the ongoing quest for efficient high-

density magnetic storage with stable magnetization and fast switching characteristics, materials with high perpendicular magnetic anisotropy and low Gilbert damping are actively sought and investigated both experimentally [11, 12] and theoretically [13]. The renewed interest in FM/HM systems is also driven by the finite Dzyaloshinskii-Moriya interaction (DMI) arising from structural inversion asymmetry, which can stabilize chiral magnetic structures [14–18]).

In theoretical calculations, the MCA energy is usually determined using the force theorem (FT) [19, 20], as the difference of occupied band energies for two different magnetization directions, calculated in the presence of the SOC, or the difference of the respective free energies (or grand potentials) at finite temperature to improve convergence [21–23]. An alternative approach to the MCA energy, proposed by Bruno [4], is based on the second-order perturbation theory (PT), with the SOC as the perturbation. It is relevant for systems with reduced symmetry, such as magnetic films and multilayers, as well as bulk crystals with a hexagonal structure or a cubic structure distorted by strain. For systems with full cubic symmetry, however, the fourth-order PT would be required but it is not used in practice.

The PT formula for the MCA energy [4, 5, 21–23] is often applied to provide insights into the electronic origin of the MCA in specific systems, particularly by identifying contributing quantum states with specific symmetries [24–31]. It can also be used to decompose the MCA energy into layer- or atom-resolved terms [26, 27, 32], although this decomposition is not unique [22] because a qualitatively different spatial distribution of this energy is obtained

* mcinal@ichf.edu.pl

based on the atom-projected density of states (DOS), within both the FT [33, 34] and PT [21] approaches. Recently, it has been shown [22, 23] that the usual PT formula for the MCA energy [4, 5, 24, 27], which includes only interband terms (from pairs of electron states), needs to be amended with intraband terms (from individual states) for systems without the inversion symmetry, such as FM/NM bilayers. In Co/Pd and Co/Cu bilayers, the net interband and intraband contributions to the MCA energy are of comparable magnitudes but opposite signs, thus largely cancelling out.

The MCA energies obtained with the FT and PT are very similar for layered systems with weak and moderate SOC strengths, such as the Co film and the Co/Cu bilayer, while minor differences are found for the Co/Pd bilayer [22, 23]. However, the discrepancy between the FT and PT results for the MCA energy becomes significant for the Co/Pt bilayer, which includes a NM layer with strong SOC. Substantial differences between the FT and PT MCA energies are also found for CoPt and FePt alloys [31, 35] as well as the thinnest Fe/Pt bilayer of 2 monolayer (ML) thickness [35].

The discrepancy between the FT and PT predictions for the Co/Pt bilayer is particularly pronounced for the oscillations of the MCA energy, with the oscillation amplitude a few times larger in the PT calculations. Oscillations of the MCA energy are predicted in numerous theoretical calculations [5, 21–23, 25, 29, 37–39, 42–44] and have also been observed in experiments for layered systems with varied thicknesses of Co, Fe, Cu, Pd and Au layers [40, 46, 48–50]. These oscillations are attributed to quantum-well (QW) d states in ferromagnetic layers of Co and Fe [38, 43, 47], and non-magnetic Pd layers [41, 42, 48], as well as to QW sp states in Cu and Au layers [40, 50].

This work aims to investigate, in depth, inaccuracies of the MCA energy calculated with the PT. To elucidate the origin of the discrepancies between the FT and PT results, the present study first examines the Co film with nominal and enhanced SOC (Sec. III A). Further (Sec. III B), the MCA oscillations versus the Co thickness are analyzed for a model subsystem of QW state pairs in the central region of the Brillouin zone (BZ) which are responsible for the dominating term of these oscillations. In the second part (Sec. III C), the MCA energies obtained with the FT and PT are examined for the Co/Pt bilayer, with a focus on the differences in their oscillations.

II. THEORY

In the presence of the SOC, the energies $\epsilon_m(\mathbf{k})$ of electron states $|m\mathbf{k}\rangle$ in a ferromagnetic film or a system with ferromagnetic and nonmagnetic layers depend on the direction of the magnetization \mathbf{M} ; for each wave vector $\mathbf{k} = (k_x, k_y)$, these states are labelled with a single band index m as the spin is no longer a good quantum number due to the SOC. With the aid of the FT, the MCA energy at zero temperature is then defined as the difference of band energies $E_b(\mathbf{M})$ [sums of the energies $\epsilon_m(\mathbf{k})$ of the occupied states] for the out-of-plane and in-plane magnetization directions, denoted

as $\hat{\mathbf{M}}_\perp$ (along the z axis) and $\hat{\mathbf{M}}_\parallel$ (along the x axis), respectively. If this approach is extended to finite temperatures the MCA energy E_{MCA} is calculated, in the canonical ensemble, as the difference $\Delta F = F(\hat{\mathbf{M}}_\perp) - F(\hat{\mathbf{M}}_\parallel)$ of the free energies for the two magnetization directions [22, 23]. The shape anisotropy energy E_{dip} due to the magnetic dipolar interaction [5] must be added to E_{MCA} to obtain the total magnetic anisotropy energy the sign of which determines the preferable direction of magnetization.

The MCA energy can also be determined within the grand canonical ensemble (cf. Ref. [21]),

$$E_{\text{MCA}} = E_{\text{MCA}}^{\text{FT}} = \Omega(\hat{\mathbf{M}}_\perp) - \Omega(\hat{\mathbf{M}}_\parallel), \quad (1)$$

where the grand potential Ω at temperature T

$$\Omega(\hat{\mathbf{M}}) = \frac{1}{N_{2D}} \sum_{m\mathbf{k}} g[\epsilon_m(\mathbf{k})] \quad (2)$$

is defined with the function $g(\epsilon) = -k_B T \ln\{1 + \exp[(\epsilon_F - \epsilon)/k_B T]\}$; here, the ϵ_F is the Fermi energy (or, more precisely, the chemical potential) and k_B denotes the Boltzmann constant. With N_{2D} equal to the number \mathbf{k} points in the two-dimensional Brillouin zone (BZ), the MCA energy is defined per primitive unit surface cell, or per surface atom for systems with one atom per a cell. The value of ϵ_F is fixed and corresponds to the number of electrons N for one of the magnetization directions, e.g., in-plane, though taking ϵ_F for the other direction gives nearly identical results for $E_{\text{MCA}}^{\text{FT}}$. The temperature T is originally introduced to improve the convergence of the integration over the BZ by smearing the Fermi level. However, this also has a physical effect by reducing the amplitude of the MCA energy oscillations with increasing the film thickness as predicted theoretically [21] and confirmed experimentally [47, 49] for Fe and Co films.

The applied definition of E_{MCA} using the grand potential [Eq. (1)] is convenient since it assumes the common Fermi level for both magnetization directions. In particular, it is suitable for the model subsystem of QW states investigated in Sec. III B 1 where the change of the Fermi energy with the magnetization direction, $\Delta\epsilon_F = \epsilon_F(\hat{\mathbf{M}}_\perp) - \epsilon_F(\hat{\mathbf{M}}_\parallel)$, would be needed as an extra external parameter (determined for the whole system) if the MCA energy was defined as the free energy difference ΔF . A similar approach, also based on the grand potential, though with $\Omega = E_b - \epsilon_F N$ at zero temperature, was successfully used to calculate the MCA energy of Co and Fe films in Refs. [33, 34]. Nevertheless, as noted therein, the MCA energies obtained with the FT in the canonical and grand canonical ensembles are (almost) the same as confirmed by the present results in Sec. III A.

Another method of calculating the MCA energy is provided by the PT with the spin-orbit interaction H_{so} treated as a perturbation in the system Hamiltonian $H + H_{\text{so}}$ where H is the unperturbed Hamiltonian describing the system in the absence of the SOC. For each electron state, its energy $\epsilon_m = \epsilon_{n\sigma}^{\text{per}} = \epsilon_{n\sigma} + \epsilon_{n\sigma}^{(1)} + \epsilon_{n\sigma}^{(2)}$ is then represented with the first-order and second-order corrections to the energy $\epsilon_{n\sigma} = \epsilon_{n\sigma}(\mathbf{k})$ of the unperturbed state $|n\sigma\mathbf{k}\rangle$ labelled with

band index n for each spin σ (\uparrow or \downarrow). In the resulting expansion of the grand potential $\Omega = \Omega_0 + \Omega^{(1)} + \Omega^{(2)}$, the first-order correction $\Omega^{(1)}$ vanishes. Indeed, for systems with the inversion symmetry, we have $\epsilon_{n\sigma}^{(1)} = 0$ at each \mathbf{k} , while, in the absence of this symmetry, although the corrections $\epsilon_{n\sigma}^{(1)}(\mathbf{k})$ can be finite, the contributions to $\Omega^{(1)}$ from \mathbf{k} and $-\mathbf{k}$ cancel out due to the relation $\epsilon_{n\sigma}^{(1)}(-\mathbf{k}) = -\epsilon_{n\sigma}^{(1)}(\mathbf{k})$ [22]. As a result, the MCA energy for layered system is given by the following second-order PT expression [21–23]

$$E_{\text{MCA}} = E_{\text{MCA}}^{\text{PT}} = \Omega^{(2)}(\hat{\mathbf{M}}_{\perp}) - \Omega^{(2)}(\hat{\mathbf{M}}_{\parallel}) \quad (3)$$

where

$$\Omega^{(2)}(\hat{\mathbf{M}}) = \frac{1}{2} \frac{1}{N_{2\text{D}}} \sum_{\mathbf{k}} \sum_{\sigma, \sigma'} \sum_{n, n'} \frac{f_0(\epsilon_{n\sigma}(\mathbf{k})) - f_0(\epsilon_{n'\sigma'}(\mathbf{k}))}{\epsilon_{n\sigma}(\mathbf{k}) - \epsilon_{n'\sigma'}(\mathbf{k})} \times |\langle n'\mathbf{k}\sigma' | H_{\text{so}} | n\mathbf{k}\sigma \rangle|^2 \quad (4)$$

is calculated with the occupation factor $f_0(\epsilon) = f(\epsilon; \epsilon_F = \epsilon_{F0})$ corresponding to the unperturbed system with the Fermi energy ϵ_{F0} . The identical corrections are found for the free energy, $F^{(1)} = \Omega^{(1)} = 0$ and $F^{(2)} = \Omega^{(2)}$ (see Appendix in Ref. 22) so that the same PT formula is obtained for the MCA energy defined as the difference of the free energies. This formula can be also represented (see, e.g., Ref. [35]) in a fully equivalent form where the ratio $\frac{1}{2}(f_{n\sigma} - f_{n'\sigma'})/(\epsilon_{n\sigma} - \epsilon_{n'\sigma'})$ [with $f_{n\sigma}$ denoting $f_0(\epsilon_{n\sigma})$] is replaced with the non-symmetrical expression $f_{n\sigma}(1 - f_{n'\sigma'})/(\epsilon_{n\sigma} - \epsilon_{n'\sigma'})$. That alternative formula reproduces Eq. (4) once the contributions from the pairs of states $(n\sigma, n'\sigma')$ and $(n'\sigma', n\sigma)$ are summed.

The MCA energy defined with Eqs. (3) and (4) is given by the sum of contributions from pairs of electrons states, with same and opposite spins,

$$E_{\text{MCA}}^{\text{PT}} = \frac{1}{2} \frac{1}{N_{2\text{D}}} \sum_{\mathbf{k}} \sum_{n\sigma, n'\sigma'} E_{\text{MCA}}^{n\sigma, n'\sigma'}(\mathbf{k}) \quad (5)$$

which results in the representation of the MCA energy as the sum of spin-pair terms

$$E_{\text{MCA}}^{\text{PT}} = \sum_{\sigma, \sigma'} E_{\text{MCA}}^{\sigma\sigma'}. \quad (6)$$

The terms with different spins, $E_{\text{MCA}}^{\downarrow\uparrow}$ and $E_{\text{MCA}}^{\uparrow\downarrow}$, comprise only interband contributions $[(n'\sigma') \neq (n\sigma)]$ while the terms with the same spins include both interband and interband $[(n'\sigma) = (n\sigma)]$ contributions,

$$E_{\text{MCA}}^{\sigma\sigma} = E_{\text{MCA},\text{inter}}^{\sigma\sigma} + E_{\text{MCA},\text{intra}}^{\sigma\sigma} \quad (7)$$

($\sigma = \downarrow$ and $\sigma = \uparrow$); see Refs. 22 and 23.

While the second-order interband terms come from electron energy corrections $\epsilon_{n\sigma}^{(2)}$ of the same order, finite second-order intraband terms $f_0'(\epsilon_{n\sigma})[\epsilon_{n\sigma}^{(1)}]^2$ originate from first-order corrections $\epsilon_{n\sigma}^{(1)} = \langle n\mathbf{k}\sigma | H_{\text{so}} | n\mathbf{k}\sigma \rangle$ in the absence of the inversion symmetry. These terms arise from the power series expansion of the $g(\epsilon_m = \epsilon_{n\sigma}^{\text{per}})$ terms of Ω [Eq. (2)]

around $\epsilon = \epsilon_{n\sigma}$ [22, 23] and reflect small shifts of the Fermi surface sheets (or rather the Fermi contour lines in two-dimensional \mathbf{k} space) due to the SOC [23]. The intraband terms are not included in the original PT formula [4] where the changes in the occupations of the electron states are neglected. However, the inclusion of such terms in the MCA energy is shown to be crucial for systems without the inversion symmetry, like Co/Cu and Co/Pd bilayers [23]. It is found that the total intraband and interband terms of this energy,

$$E_{\text{MCA},\text{intra}} = E_{\text{MCA},\text{intra}}^{\downarrow\downarrow} + E_{\text{MCA},\text{intra}}^{\uparrow\uparrow} \quad (8)$$

and

$$E_{\text{MCA},\text{inter}} = E_{\text{MCA},\text{inter}}^{\downarrow\downarrow} + E_{\text{MCA},\text{inter}}^{\uparrow\uparrow} + E_{\text{MCA}}^{\downarrow\uparrow} + E_{\text{MCA}}^{\uparrow\downarrow}, \quad (9)$$

respectively, are of comparable magnitude, though of opposite signs, so that they largely cancel out in the sum

$$E_{\text{MCA}}^{\text{PT}} = E_{\text{MCA},\text{intra}} + E_{\text{MCA},\text{inter}} \quad (10)$$

which gives the total MCA energy in the PT approach.

The intraband terms of the MCA energy differ from the unconventional second-order terms identified in Refs. 51 and 52. Although they both come from changes of electron energies linear in the SOC strength and are localized along lines in the BZ, the latter terms do not originate from the first-order PT corrections $\epsilon^{(1)}$. Furthermore, unlike the intraband terms, they are not related to the lack of the inversion symmetry. Instead, they arise under specific conditions: when two energy bands are degenerate near the Fermi level along a line in the \mathbf{k} space with no or very weak dispersion along that line. Then, if this degeneracy is lifted by the SOC for only one of the two magnetization directions, it results in a second-order contribution to the MCA energy from a narrow stripe-shaped region around the line. In contrast, the intraband contributions to the MCA energy arise from each band that intersects the Fermi level. This occurs at \mathbf{k} points which form a line, the respective line of the Fermi contour in the two-dimensional BZ. Formation of the Fermi contour in thin films, represented by a set of discrete lines, can also be illustrated by discretization of the bulk Fermi surface into multiple circular lines within a free-electron model, as described in Ref. 53.

The spin-orbit interaction is given by the following sum over sites j in atomic layers l of constituent transition metals with the SOC constants ξ_l ,

$$H_{\text{so}} = \sum_{lj} \xi_l \mathbf{L}(\mathbf{r} - \mathbf{R}_{lj}) \cdot \mathbf{S}. \quad (11)$$

It includes the operator of electron spin \mathbf{S} and the operators of orbital angular momentum $\mathbf{L}(\mathbf{r} - \mathbf{R}_{lj})$ which depend on the electron position \mathbf{r} with respect to the consecutive atomic locations \mathbf{R}_{lj} . Although the SOC operator itself does not depend on the direction of the magnetization, such dependence arises [3, 22, 54] when this operator is applied to the electron states $\psi(\mathbf{r}) = \psi^{\uparrow}(\mathbf{r})|\uparrow\rangle + \psi^{\downarrow}(\mathbf{r})|\downarrow\rangle$ represented with two spatial wave functions $\psi^{\uparrow}(\mathbf{r})$ and $\psi^{\downarrow}(\mathbf{r})$ in

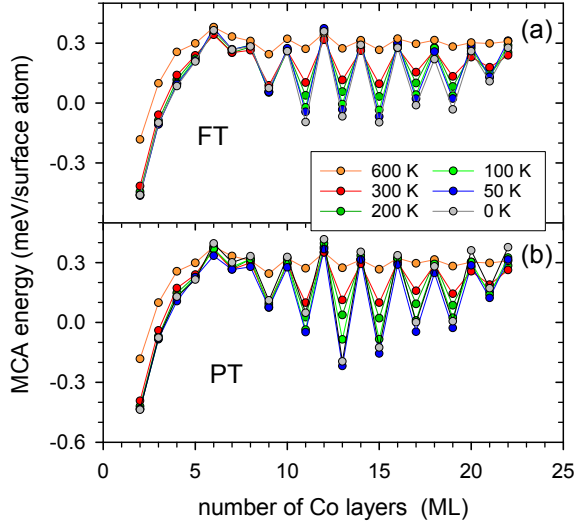


FIG. 1: MCA energy of the (001) fcc Co film with the nominal SOC strength ($\xi = \xi_{\text{Co}}$) calculated with (a) the FT and (b) the PT at various temperatures.

the spin basis $|\sigma\rangle$ ($\sigma = \uparrow, \downarrow$) corresponding to the eigenstates of the operator S_{ζ} of spin component along the magnetization direction $\hat{\mathbf{M}}$. The spin operator is then represented as $\mathbf{S} = (S_{\xi}, S_{\eta}, S_{\zeta})$ in the rotated frame of reference $O\xi\eta\zeta$ with the ξ and η axes perpendicular to the spin quantization axis ζ while the fixed frame of reference $Oxyz$ is used for $\mathbf{L} = (L_x, L_y, L_z)$ and linked to the system geometry with the z axis oriented perpendicular to the film surface and the x and y axes parallel to it. For the considered (001) fcc films, the x , y and z axes are along (100), (010), and (001) crystallographic directions, respectively.

The electronic structure is described using a realistic TB model, with nine basis orbitals (per atom) of s , p and d symmetries for each spin σ and hopping parameters fitted to ab initio bulk bands [55]. The applied model also includes shifts of on-site orbital energies, to make each atomic layer electrically neutral and account for different orientations of orbitals at surfaces and interfaces, as well as local exchange splittings self-consistently adjusted to layer magnetic moments. The details of this TB model are described in Refs. 22, 38, and 42.

The use of a TB model in the custom-built code allows for efficient calculations of the MCA energy in thick layered systems in both the FT and PT approaches and targeted analysis of the obtained results, with modest computer resources. The 0.01 meV accuracy of the MCA energy is reached at $T = 300$ K with a moderate number $N_{2D} = (2N_k + 1) \times (2N_k + 1) \approx 3700$ of \mathbf{k} points using a square mesh with $N_k = 30$, while larger numbers of \mathbf{k} points are needed for convergence at lower temperatures, up to $N_{2D} \approx 40000$ ($N_k = 100$) for $T = 50$ K (see Ref. 23). The calculations of the MCA energy are also done for zero temperature, using the triangle method based on division of the BZ into a triangular mesh and linearization of electron energies within each triangle. The

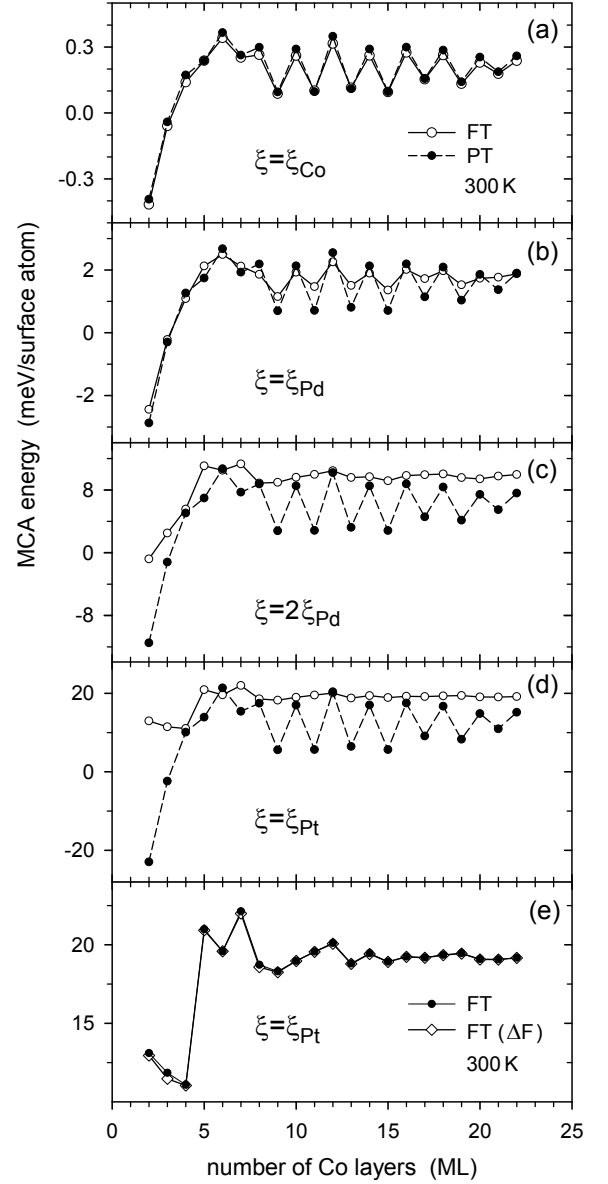


FIG. 2: MCA energy of the (001) fcc Co film calculated with (a-e) the FT [Eq. (1)] and (a-d) the PT [Eq. (3)] for various strengths ξ of the SOC coupling at $T = 300$ K. For comparison, the results of the alternative FT formula $\Delta F = F(\mathbf{M}_{\perp}) - F(\mathbf{M}_{\parallel})$ for $\xi = \xi_{\text{Pt}}$ at the same T are also shown in panel (e).

triangle formula for interband contributions in the PT approach is derived in Ref. 5. The intraband term of the MCA energy at $T = 0$ is given by a sum of the Dirac delta functions $\lim_{T \rightarrow 0} f_0^{\epsilon}(\epsilon_{n\sigma}) = -\delta(\epsilon_{n\sigma} - \epsilon_{F0})$ multiplied by the squares of $\langle n\mathbf{k}\sigma | H_{\text{so}} | n\mathbf{k}\sigma \rangle$. Accordingly, the triangle method for the projected DOS [56] can be readily adopted for numerical integrations of such intraband contributions [23]. In the FT approach, the grand potential $\Omega = E_b - \epsilon_F N$ is calculated with the analytical formula for the integral $\Omega = \int_{-\infty}^{\epsilon_F} (\epsilon - \epsilon_F) n(\epsilon) d\epsilon$ where the DOS $n(\epsilon)$ is also determined with the triangle method [57]. The square

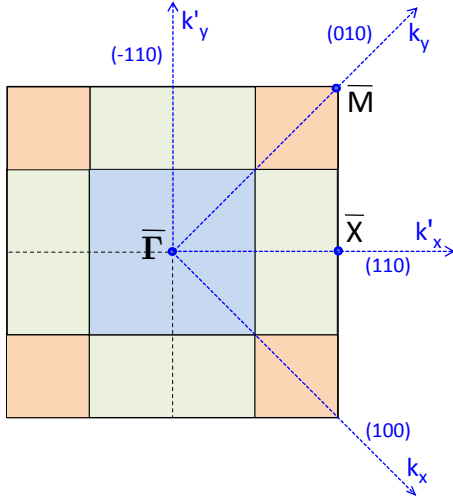


FIG. 3: Division of the BZ into the $\bar{\Gamma}$ region (blue), the \bar{M} region (orange), and the \bar{X} region (green), centred around the respective high-symmetry and equivalent \mathbf{k} -points.

mesh of \mathbf{k} points with $N_k = 100$ and each square divided into two triangles is found sufficient for convergence in both the FT and PT calculations at zero temperature.

III. RESULTS AND DISCUSSION

A. Magnetocrystalline anisotropy of Co film with enhanced spin-orbit coupling. Effect of temperature

Validity of the PT in calculations of the MCA energy and possible inaccuracies of this method are conveniently investigated for a simple ferromagnetic system of the (001) fcc Co film with a modified strength ξ of the SOC. The effect of temperature on the deviations of the PT predictions from the exact results of the FT calculations is also studied. For a fcc Co film with the nominal SOC constant ($\xi = \xi_{\text{Co}}$), it is found (Fig. 1) that the MCA energies obtained with the FT and PT are almost identical at $T = 300$ K but differ significantly when the temperature becomes low enough. At $T = 50$ and 100 K, the oscillations of the MCA energy with increasing the Co film thickness N_{Co} have significantly larger amplitude in the PT approach than in the FT calculation.

To test the effect of the SOC strength we consider Co films with the nominal SOC constant $\xi_{\text{Co}} = 0.085$ eV, as well as that of Pd $\xi = \xi_{\text{Pd}} = 0.23$ eV, its double $\xi = 2\xi_{\text{Pd}} = 0.46$ eV, and finally the SOC constant of Pt $\xi = \xi_{\text{Pt}} = 0.65$ eV [22, 58]. The MCA energies for such systems are determined with both the FT and the PT at $T = 300$ K. It is found (Fig. 2) that the PT reproduces the FT result for E_{MCA} very well only for $\xi = \xi_{\text{Co}}$ while significant discrepancies between the PT and FT predictions for the MCA energy are present for the films with the stronger SOC. This particularly concerns the oscillatory variation of E_{MCA} with increasing the Co film thickness N_{Co} . For $\xi = \xi_{\text{Pd}}$, the amplitude of the dominating oscillations

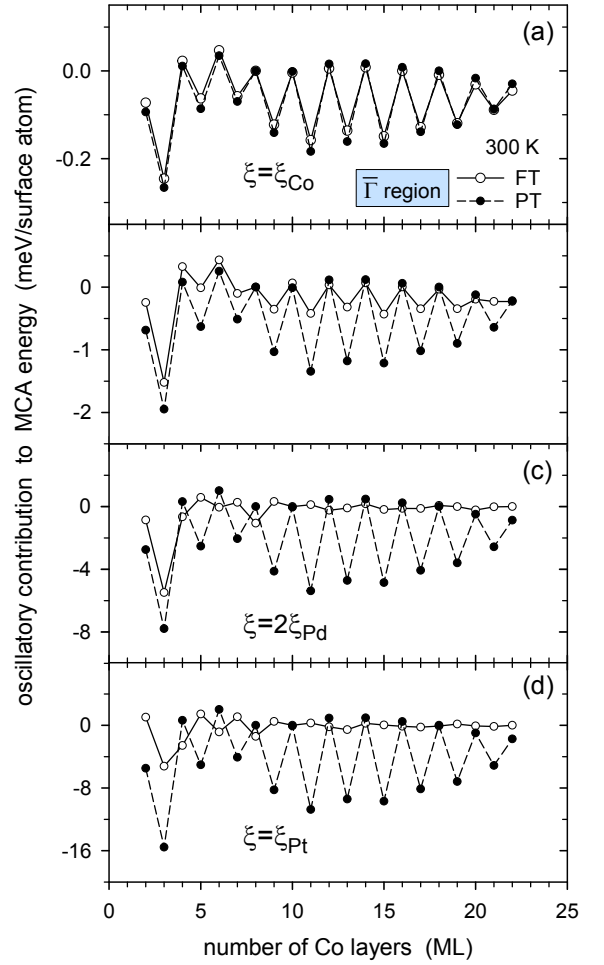


FIG. 4: (a-d) Oscillatory component of the contribution to the MCA energy from the $\bar{\Gamma}$ region in the BZ (Fig. 3), calculated with the FT and the PT for the (001) fcc Co film with various SOC strengths ξ at $T = 300$ K.

with the 2 ML period is over two times larger in the PT calculations than when using the FT. Further, for the two largest SOC constants, $\xi = 2\xi_{\text{Pd}}$ and $\xi = \xi_{\text{Pt}}$, the oscillations of the MCA energy calculated with the PT are very large compared to those in the FT approach. This implies that the oscillation amplitude obtained with the FT for strong SOC does not follow the ξ^2 dependence predicted by the PT for the MCA energy.

However, if we focus on the upper envelope of the oscillatory variation, the magnitudes of the corresponding MCA energies obtained with the FT and the PT show good agreement even for strong SOC (Fig. 2). Thus, the total MCA energy (its upper envelope) in the FT approach scales as ξ^2 , in contrast to its oscillations at large ξ . The choice of the upper envelope is dictated by the fact that, within the PT calculations, the 2 ML period oscillations of the MCA energy $E_{\text{MCA}}^{\text{PT}} = \Omega^{(2)}(\mathbf{M}_{\perp}) - \Omega^{(2)}(\mathbf{M}_{\parallel})$ in the Co film originate from the *negative* contributions to $\Omega^{(2)}$ for $\mathbf{M} = \mathbf{M}_{\perp}$ which arise from QW states crossing the Fermi level [38, 47]. These contributions, which determine the position of the

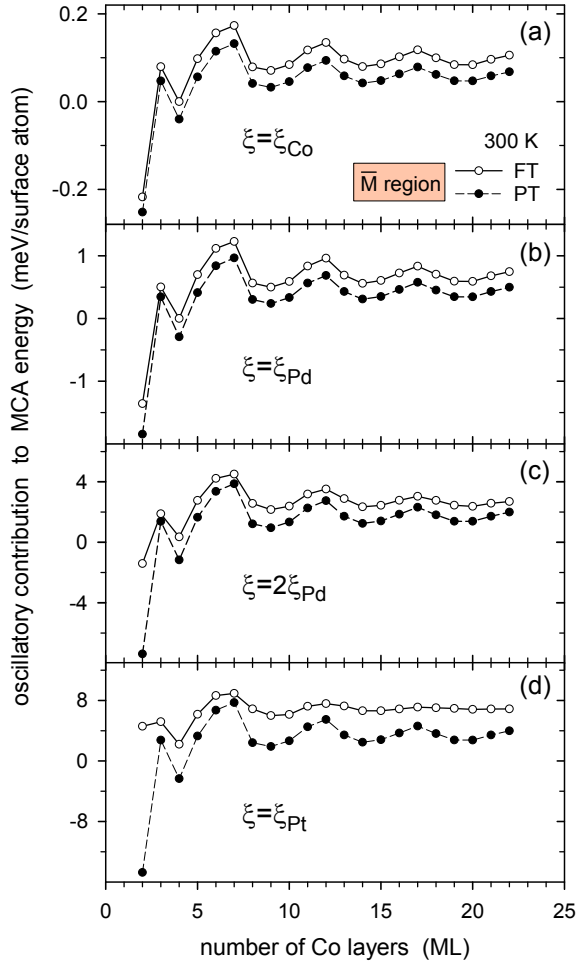


FIG. 5: (a-d) Oscillatory component of the contribution to the MCA energy from the \bar{M} region in the BZ (Fig. 3), calculated with the FT and the PT for the (001) fcc Co film with various SOC strengths ξ at $T = 300$ K. The FT and PT plots are vertically shifted with respect to each other for easier comparison. In each panel, the energy scale is the same as in Fig. 4.

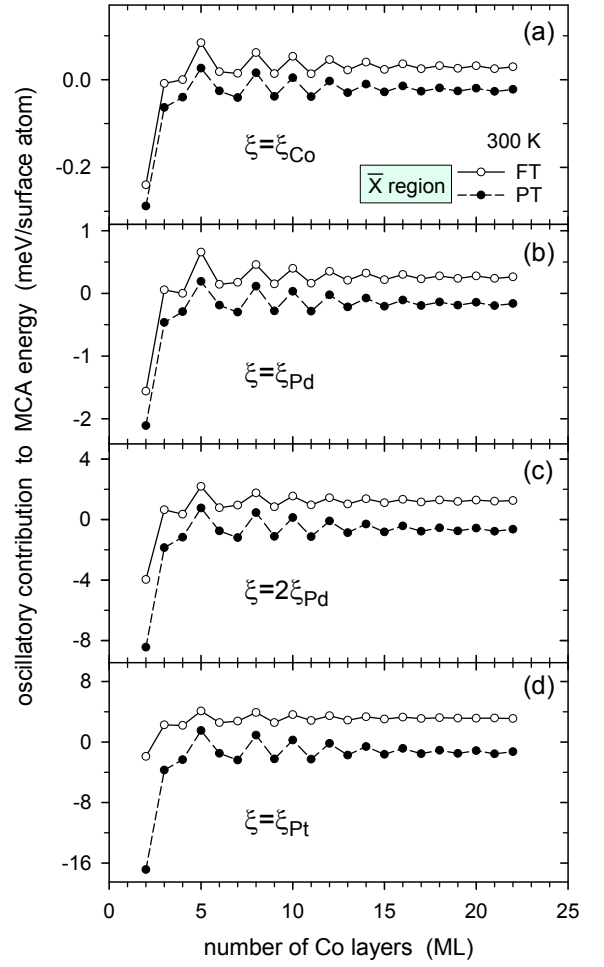


FIG. 6: (a-d) Oscillatory component of the contribution to the MCA energy from the \bar{X} region in the BZ (Fig. 3), calculated with the FT and the PT for the (001) fcc Co film with various SOC strengths ξ at $T = 300$ K. The FT and PT plots are vertically shifted with respect to each other for easier comparison. In each panel, the energy scale is the same as in Fig. 4.

lower envelope in the $E_{MCA}^{PT}(N_{Co})$ variation, become smaller with increasing temperature. Consequently, the corresponding MCA oscillations become smaller while the upper envelope of $E_{MCA}^{PT}(N_{Co})$ remains almost unchanged; see Fig. 1.

Note also that the MCA energies obtained with the FT using the grand potential Ω [Eq. (1)] are almost identical to the respective MCA energies defined, also within the FT approach, as the free energy difference ΔF . This is illustrated for the Co film with the SOC of Pt in Fig. 2(e), where the difference between the results of the two types of the FT calculations is hardly noticeable while for weaker SOC these two MCA energies are indistinguishable in the scales of Fig. 2(a)-(c).

To further analyze the described discrepancies between the FT and PT results at different strengths of the SOC we examine the contributions to the MCA energies from three different regions of the two-dimensional BZ which are

centred (if viewed in the extended BZ picture) around the high-symmetry points, $\bar{\Gamma}$, \bar{M} and \bar{X} , correspondingly (Figs. 3, 4, 5, 6). As previously established [38], the oscillations of the 2 ML period which dominate in the variation of the MCA energy at the nominal SOC strength of Co both within the PT and FT approaches come from the central region of the BZ around the $\bar{\Gamma}$ point. In the PT approach, oscillations from this $\bar{\Gamma}$ region are also predominant at stronger SOC, since they scale as ξ^2 , but they are much smaller in the FT calculations and no longer dominate. Accordingly, all three parts of the BZ then contribute significantly to the oscillatory pattern of $E_{MCA}^{FT}(N_{Co})$, with terms of different periods and similar amplitudes. The region around the \bar{M} point (\bar{M} region) contributes to the thickness variation of the MCA energy with an oscillatory term of 5.15 ML period which comes from the QW states derived from the bulk band of the Z_3 symmetry [38]. This term is very similar in the PT

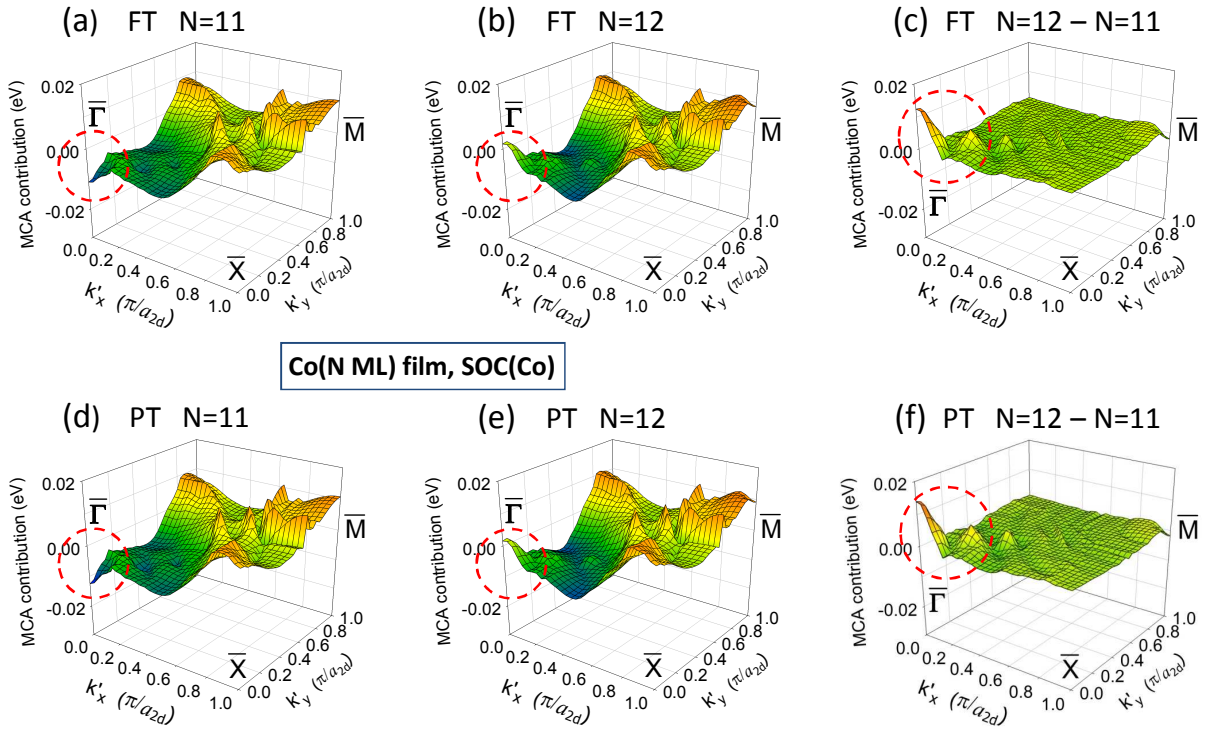


FIG. 7: Distribution of MCA energy in the BZ for the fcc (001)(a,d) Co(11 ML) and (b,e) Co(12 ML) films with the nominal SOC strength ($\xi = \xi_{\text{Co}}$) at $T = 300$ K, obtained with the FT (top row) and the PT (bottom row). (c,f) Difference between the 12 ML and 11 ML distributions. The plots show the symmetrized distributions in one quarter of the BZ (see Appendix A).

and FT approaches not only for $\xi = \xi_{\text{Co}}$ but also for $\xi = \xi_{\text{Pd}}$, while its oscillation amplitude is significantly smaller in the FT approach only for $\xi = \xi_{\text{Pt}}$. Lastly, similar conclusions hold for the contributions from the region around the \bar{X} point, the \bar{X} region. Thus, it is found that the discrepancy between the MCA energies obtained with the PT and FT originates mainly from the $\bar{\Gamma}$ region.

These findings are visualized with the plots of the MCA energy distributions within the BZ (Figs. 7 and 8). For Co films with the nominal SOC ($\xi = \xi_{\text{Co}}$), the distributions calculated with the FT and PT are nearly identical. However, a significant difference emerges at strong SOC. The peaky features in the PT distribution of E_{MCA} in some regions of the BZ are largely smoothed out in the FT distribution for the SOC of Pt. Specifically, the PT predicts, for any SOC strength, regular changes in the MCA energy contributions around the $\bar{\Gamma}$ point with increasing the Co thickness (from $N_{\text{Co}} = 11$ to 12 ML in Figs. 7 and 8), leading to 2 ML period oscillations. These changes are barely present in the FT distribution at strong SOC. This is particularly evident in the difference between the MCA energy distributions in the Co(12 ML) and Co(11 ML) films which represents the distribution of the oscillation amplitude; see Figs. 7 (c), (f) and 8 (c), (f). The amplitude distribution is nearly flat in the FT calculations for the SOC of Pt, while being almost identical to the respective PT distribution for the SOC of Co. Nevertheless, if the rapid variations of MCA contribu-

tions within the BZ are disregarded, the overall shapes of the MCA energy distributions are similar in the FT and PT approaches for all considered SOC strengths.

B. Why perturbation theory fails for magnetocrystalline energy oscillations at strong spin-orbit coupling

1. Model subsystem of quantum-well states that come in pairs

The 2 ML period oscillations of the MCA energy in the (001) fcc Co film come from pairs of QW states which, in the absence of the SOC, are degenerate at the very centre of the BZ, the $\bar{\Gamma}$ point [$\mathbf{k} = (0, 0)$], and originate from the minority-spin band of the Δ_5 symmetry in bulk fcc Co [38]. Such pairs of QW states can be identified in the unperturbed band structure of the (001) fcc Co film by projecting the quantum states with \mathbf{k} close to $\bar{\Gamma}$ onto the (yz, zx) orbital subspace; see Fig. 9. The energies of these states shift as the Co thickness increases. As a result, the Fermi energy is close to the energies of a QW state pair for some thicknesses, such as $N_{\text{Co}} = 11, 13$, and 15 ML, but lies between the energies of two neighboring pairs for other thicknesses, such as $N_{\text{Co}} = 10, 12$, and 14 ML. Such regular energy shifts give rise to an oscillatory contribution to the MCA energy from the $\bar{\Gamma}$ region, as predicted by the PT formula, Eq. (3). Within the FT approach, the contribution to the

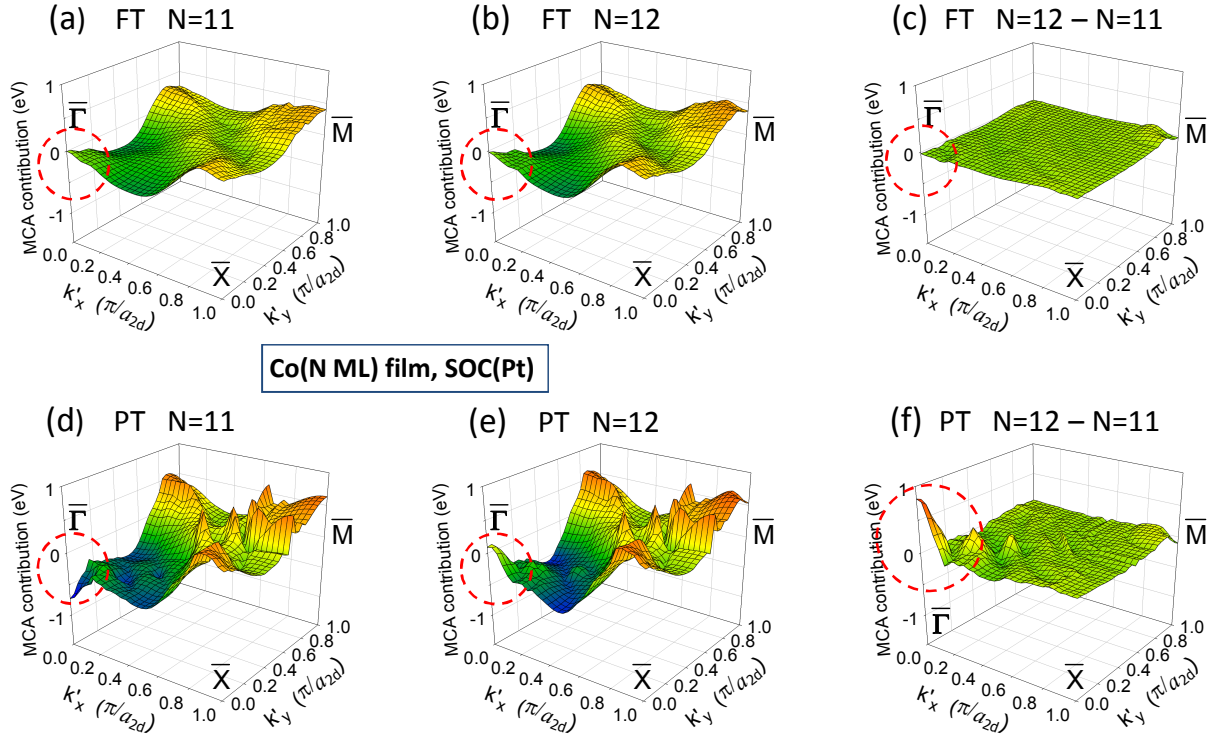


FIG. 8: Distribution of MCA energy in the BZ for the fcc (001) (a,d) Co(11 ML) and (b,e) Co(12 ML) films with the SOC strength of Pt ($\xi = \xi_{\text{Pt}}$) at $T = 300$ K, obtained with the FT (top row) and the PT (bottom row). (c,f) Difference between the 12 ML and 11 ML distributions. The plots show the symmetrized distributions (see Appendix A).

MCA energy from the QW states in the $\bar{\Gamma}$ region arises from differences in the electron energy bands for the two magnetization directions and this contribution can oscillate as the energies of the perturbed QW states shift with increasing the film thickness. For the in-plane magnetization, the energy bands around the $\bar{\Gamma}$ point are only slightly modified by the SOC, as illustrated in Fig. 10. In contrast, significant energy splittings of electron occur for the QW states at $\mathbf{k} = (0, 0)$ and near this point for the out-of-plane magnetization.

To further investigate the possibly different predictions of the FT and PT for the MCA energy oscillations, a simple model can be used which approximates the MCA contributions from the specified pairs of minority-spin QW states. In the absence of the SOC, the two states in each pair (labelled with index p) are degenerate at $\mathbf{k} = (0, 0)$, both having the energy $\epsilon_{0,p}$, and their energies change quadratically with the distance $k = |\mathbf{k}| = \sqrt{k_x^2 + k_y^2}$ from the centre of the BZ:

$$\epsilon_{1,p}(k) = \epsilon_{0,p} + b_1 k^2, \quad (12)$$

$$\epsilon_{2,p}(k) = \epsilon_{0,p} + b_2 k^2. \quad (13)$$

The dispersion parameters b_1 and b_2 ($b_2 > b_1$) depend on the direction of \mathbf{k} , i.e., the angle $\phi = \arctan(k_y/k_x)$ so they are constant along each line starting at $\bar{\Gamma}$. Deviations from the quadratic dependence are neglected because, as shown in Fig. 9, they are not significant in the interval $0 \leq k \lesssim 0.1\pi/a_{2d}$ where the MCA oscillatory contributions

with the 2 ML period arise (Figs. 7 and 8). Here, the lattice constant $a_{2d} = a/\sqrt{2}$ corresponds to the two-dimensional square lattice of the (001) fcc surface (a is the fcc lattice constant).

The considered states are built of yz and zx orbitals,

$$\psi_{1,p}(\mathbf{k}) = c|p\mathbf{k}yz\downarrow\rangle - d|p\mathbf{k}zx\downarrow\rangle \quad (14)$$

$$\psi_{2,p}(\mathbf{k}) = d|p\mathbf{k}yz\downarrow\rangle + c|p\mathbf{k}zx\downarrow\rangle, \quad (15)$$

they are orthogonal and normalized ($c^2 + d^2 = 1$, c and d can be chosen real [41]). Their components $|p\mathbf{k}\mu\sigma\rangle = \mathcal{N} \sum_l \sin(k_{z,p} z_l) |k_l\mu\sigma\rangle$ are the two-dimensional Bloch states built of the orbitals μ (yz and xz) with spin $\sigma = \downarrow$, located at position $z_l = la/2$ in each layer l and normalized with the factor \mathcal{N} . The actual composition of these states depends on the direction of the \mathbf{k} vector, with $c = d = 1/\sqrt{2}$ for $k_x = k_y$ (along the $\bar{\Gamma} - \bar{X}$ line) and $c = 0, d = 1$ for $k_x = 0$ (along the $\bar{\Gamma} - \bar{M}$ line). For simplicity, it is assumed that the coefficients c and d depend so slowly on the distance $k = |\mathbf{k}|$ from the centre of the BZ that this dependence can be neglected altogether. Contributions from other orbitals are also neglected, in agreement with the near-unity projections ($P_1 \approx 1$ and $P_2 \approx 1$) of the QW states in the Co film onto the corresponding orthogonal combinations

$$|\phi_1\rangle = c|yz\rangle - d|zx\rangle, \quad (16)$$

$$|\phi_2\rangle = d|yz\rangle + c|zx\rangle \quad (17)$$

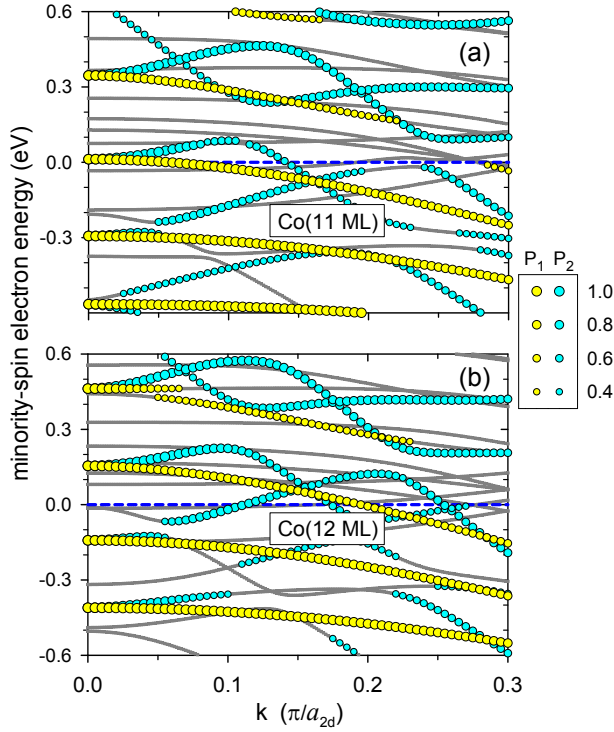


FIG. 9: Minority-spin electron energies along the $\bar{\Gamma} - \bar{X}$ line near the BZ centre for the (001) fcc Co(11 ML) and Co(12 ML) films without the SOC. The colour-marked bands correspond to the states with projections $P_1 \geq 0.4$ onto the $|\phi_1\rangle = (|yz\rangle - |zx\rangle)/\sqrt{2}$ orbitals (yellow circles), and $P_2 \geq 0.4$ onto the $|\phi_2\rangle = (|yz\rangle + |zx\rangle)/\sqrt{2}$ orbitals (light blue circles); P_1 and P_2 are equal to 1 at $k = 0$. The Fermi energy is at $\epsilon_{F0} = 0$ (horizontal dashed line).

of the yz and zx orbitals; see Fig. 9.

The different pairs of the QW states $\psi_{j,p}$ with energies $\epsilon_{j,p}$ ($j = 1, 2$) correspond to different energies $\epsilon_{0,p}$ and discrete values of $k_z = k_{z,p} \approx \pi p / [(N_{\text{Co}} + 1)d]$ where $p = 1, \dots, N_{\text{Co}}$ and $d = a/2$. This arises from the quantization of the z -component of the three-dimensional wave vector (\mathbf{k}, k_z) in the QW of the film. The energy $\epsilon_{0,p}$ of the p -th pair QW states at $\mathbf{k} = (0, 0)$ can be approximated by the energy $\epsilon_{n\downarrow}^{\text{bulk}}(\mathbf{k}, k_z)$ of the minority-spin Δ_5 bulk band at the $(0, 0, k_z = k_{z,p})$ point. For the QW states with $\epsilon_{0,p}$ close to the Fermi energy, the values of $k_{z,p}$ are close to the extremal radius of the Fermi surface sheet of this bulk band, which determines the oscillation period of 2.12 ML associated with the considered QW states [38].

The model system comprises several QW state pairs ($p = 1, 2, \dots, P$), with energies $\epsilon_{0,p}$ at $\mathbf{k} = (0, 0)$ separated by $\Delta\epsilon_0$ from each other, as illustrated in Fig. 11. The assumed values of $\Delta\epsilon_0 = 0.3$ eV and the dispersion parameters b_1 and b_2 , are fitted to the energy bands near the Fermi energy in the Co(12 ML) film (Fig. 9). For thicker films, the spacing $\Delta\epsilon_0$ between the neighboring pairs decreases due to finer quantization of $k_z = k_{z,p}$. The considered subsystem can be limited to a few QW state pairs (even $P = 7$ in the

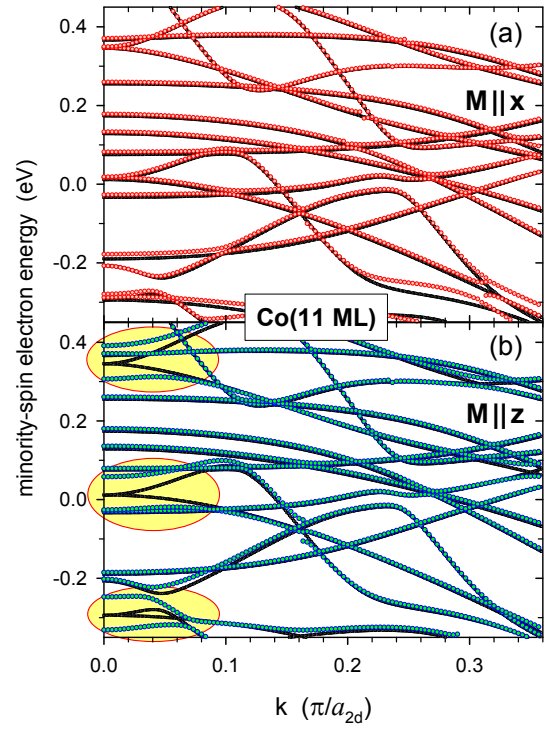


FIG. 10: (a,b) Electron energies along the $\bar{\Gamma} - \bar{X}$ line near the BZ centre for the (001) fcc Co(11 ML) film: minority-spin energies in the film without the SOC (black lines) and the energies of states with a dominating minority-spin component (with a probability larger than 0.5) calculated with the nominal SOC ($\xi = \xi_{\text{Co}}$) for the (a) in-plane magnetization $\mathbf{M} \parallel x$ (red circles) and (b) out-of-plane magnetization $\mathbf{M} \parallel z$ (green circles). The yellow ovals highlight pairs of states which are built predominantly of the yz and zx orbitals and are split by the SOC for $\mathbf{M} \parallel z$.

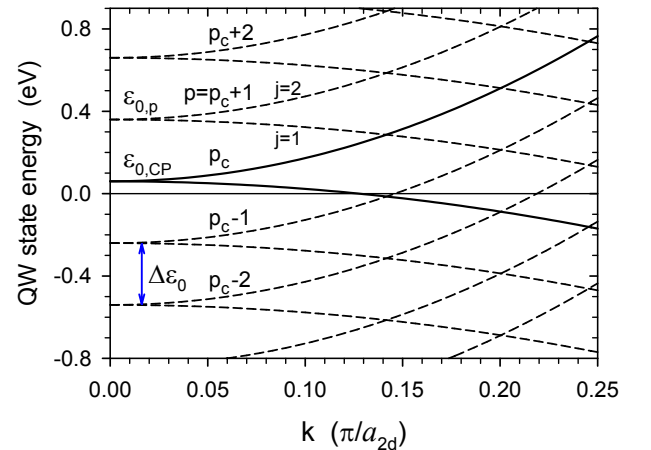


FIG. 11: Energies $\epsilon_{j,p}$ ($j = 1, 2$ and $p = p_c, p_c \pm 1, p_c \pm 2, \dots$) of model QW state pairs in the Co film in the absence of the SOC [Eqs. (12) and (13)] versus $k = |\mathbf{k}|$ along the $\bar{\Gamma} - \bar{X}$ line. The index $p = p_c$ denotes the central QW state pair with the energy $\epsilon_{0,\text{CP}}$ at $k = 0$ (here 0.06 eV). The Fermi energy is at $\epsilon_{F0} = 0$ (horizontal line).

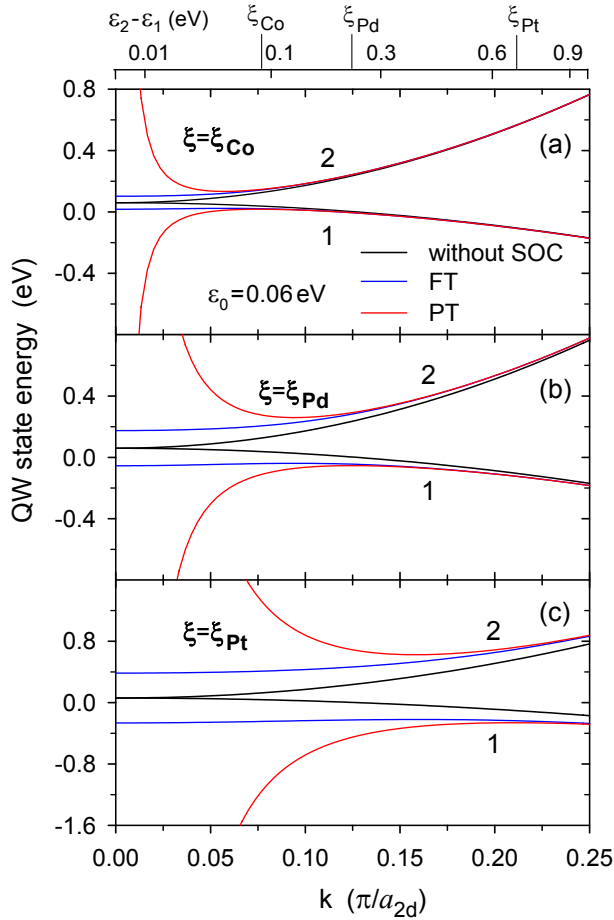


FIG. 12: Energies $\epsilon_{1,p}$ and $\epsilon_{2,p}$ of a model QW state pair [Eqs. (12) and (13)] with $\epsilon_{0,p} = 0.06$ eV in the Co film without the SOC (black lines) versus $k = |\mathbf{k}|$ along the $\bar{\Gamma} - \bar{X}$ line; $\epsilon_{F0} = 0$. Corresponding energies $\epsilon_{1,p}^{\text{FT},\perp}$ and $\epsilon_{2,p}^{\text{FT},\perp}$ (blue lines), and $\epsilon_{1,p}^{\text{PT},\perp}$ and $\epsilon_{2,p}^{\text{PT},\perp}$ (red lines) for the out-of-plane direction of magnetization, obtained using the FT and the PT, respectively, with the SOC constants of (a) Co, (b) Pd, and (c) Pt; see Eqs. (21) and (23). The top scale shows the energy separation $\Delta\epsilon = \epsilon_{2,p} - \epsilon_{1,p}$ in each pair of QW states, with the marked values of the SOC constants.

present calculations) since pairs with energies far from the Fermi level give negligible contributions to the MCA energy. This is because the respective terms in Ω are either very small or finite but nearly identical for the in-plane and out-of-plane magnetizations so they cancel out.

A key parameter that affects the MCA energy of this subsystem is the energy $\epsilon_{0,\text{CP}} = \epsilon_{0,p}$ of the QW state pair at $\mathbf{k} = (0, 0)$ which is closest to the Fermi level. This pair is hereafter referred to as the *central pair* of QW states with index $p = p_c$. Accordingly, the energies $\epsilon_{0,p}$ of other pairs at $k = 0$ (where $\epsilon_{1,p} = \epsilon_{2,p}$) are shifted with respect to $\epsilon_{0,\text{CP}}$ by the $\Delta\epsilon_0$ spacing or its multiples, i.e., they are equal to $\epsilon_{0,p} = \epsilon_{0,\text{CP}} + (p - p_c)\Delta\epsilon_0$ where $p = p_c \pm 1, p_c \pm 2, \dots$. The zero energy level of $\epsilon_{0,\text{CP}} = 0$ corresponds to the Fermi

energy $\epsilon_{F0} = 0$. For simplicity, the same value $\epsilon_F = 0$ of the Fermi energy is assumed in the model of QW states for the perturbed system. The effects of a possible shift of the Fermi energy due to the SOC perturbation are discussed in the last part of Sec. III B 2.

In each pair, both QW states $\psi_{1,p}$ and $\psi_{2,p}$ are of the same spin ($\sigma = \downarrow$) so the matrix elements of the SOC operator $\langle \psi_{i,p} | H_{\text{SO}} | \psi_{j,p} \rangle$ ($i, j = 1, 2$) reduce to

$$\langle \psi_{i,p} | H_{\text{SO}} | \psi_{j,p} \rangle = -\frac{1}{2}\xi \langle \phi_i | L_\zeta | \phi_j \rangle \quad (18)$$

where ζ denotes the direction of the film magnetization (the net spin). For ϕ_1 and ϕ_2 defined in Eqs. (17), all four matrix elements (18) vanish for the in-plane magnetization ($\zeta = x$ or y). This can be immediately shown when L_x and L_y are represented as linear combinations of the ladder operators L_+ and L_- , and the orbitals $|yz\rangle = (i/\sqrt{2})(|2, -1\rangle + |2, 1\rangle)$ and $|zx\rangle = (1/\sqrt{2})(|2, -1\rangle - |2, 1\rangle)$ are expressed in terms of the eigenstates $|L, m\rangle$ of \mathbf{L}^2 and L_z (where L is the orbital quantum number and m is the magnetic quantum number). The diagonal elements $\langle \psi_{j,p} | H_{\text{SO}} | \psi_{j,p} \rangle$ ($j = 1, 2$) of the SOC operator also vanish for the out-of-plane orientation of magnetization, with $L_\zeta = L_z$. However, the off-diagonal element $\langle \psi_{1,p} | H_{\text{SO}} | \psi_{2,p} \rangle$ is finite for $\zeta = z$ and equals to $-\frac{1}{2}i\xi$, independently of the direction of the \mathbf{k} vector as it is proportional to $c^2 + d^2 = 1$.

The matrix of the full Hamiltonian $H = H_0 + H_{\text{SO}}$ is block diagonal, with 2×2 blocks corresponding to individual QW state pairs. This is so because the matrix elements of both H_0 and H_{SO} between the QW states $\psi_{j,p}$ and $\psi_{j',p'}$ from different pairs ($p \neq p'$) vanish since such states are orthogonal due to different $k_{z,p}$ and $k_{z,p'}$ [38, 41]. For each pair, the Hamiltonian matrix $H_{ij} = \langle \psi_{i,p} | H | \psi_{j,p} \rangle$ ($i, j = 1, 2$) takes the following form

$$\begin{bmatrix} H_{11} & H_{12} \\ H_{21} & H_{22} \end{bmatrix} = \begin{bmatrix} \epsilon_{1,p} & V \\ V^* & \epsilon_{2,p} \end{bmatrix}. \quad (19)$$

with $V = (H_{\text{SO}})_{12} = \langle \psi_{1,p} | H_{\text{SO}} | \psi_{2,p} \rangle$. For the in-plane magnetization, corresponding to $V = 0$, the QW states are not perturbed by the SOC and their energies remain unchanged,

$$\epsilon_{j,p}^{\text{FT},\parallel} = \epsilon_{j,p} \quad (j = 1, 2). \quad (20)$$

However, this is not the case for the energies of the QW states at the out-of-plane magnetization,

$$\epsilon_{j,p}^{\text{FT},\perp} = \frac{1}{2}(\epsilon_{1,p} + \epsilon_{2,p}) \mp \frac{1}{2}\sqrt{(\Delta\epsilon)^2 + \xi^2} \quad (21)$$

(where $\Delta\epsilon = \epsilon_{2,p} - \epsilon_{1,p}$), which are obtained by the diagonalizing the pair Hamiltonian with the finite term $V = -\frac{1}{2}i\xi$. Here and in the following discussion, the plus and minus signs correspond to the lower state ($j = 1$) and the upper ($j = 2$) state in each pair, respectively. This exact solution, obtained through the diagonalization, is used in the FT approach for the simplified model of the QW states. It reproduces, with good accuracy, the splittings of the QW

state energies around the centre of the BZ that arise due to the SOC in the band structure of the full Co film system; see Figs. 10 and 12. In particular, the model predicts that the energies for the out-of-plane magnetization are split as follows at $\mathbf{k} = (0, 0)$,

$$\epsilon_{j,p}^{\text{FT},\perp}(k=0) = \epsilon_{0,p} \mp \frac{1}{2}\xi, \quad (22)$$

and they remain almost constant in a central region of the BZ where $\Delta\epsilon$ is smaller than $\xi/2$.

It is also possible to find an approximate solution for the energies of the perturbed QW states,

$$\epsilon_{j,p}^{\text{PT},\perp} = \epsilon_{j,p} \mp \frac{\xi^2}{4\Delta\epsilon}, \quad (23)$$

where the second-order correction is obtained using the PT in a similar way as in calculations of the total MCA energy with Eqs. (3) and (4). This expression can also be derived by expanding $\epsilon_{j,p}^{\text{FT},\perp}$ in powers of ξ^2 , up to the linear term. The PT solution well reproduces the exact (FT) energies for $\Delta\epsilon \geq \xi$ but becomes largely inaccurate for $\Delta\epsilon$ smaller than $\xi/2$, with the difference $\epsilon_{j,p}^{\text{PT},\perp} - \epsilon_{j,p}^{\text{FT},\perp}$ ($j = 1, 2$) equal to $\mp 0.0429\xi$ at $\Delta\epsilon = \xi$, $\mp 0.1910\xi$ at $\Delta\epsilon = \xi/2$, and $\mp 0.6096\xi$ at $\Delta\epsilon = \xi/4$. This is illustrated in Fig. 12 which shows the energies of a pair of QW states calculated using the FT and the PT for various SOC strengths and plotted as functions of k . The values of the respective SOC constants are marked on the top scale that indicates the energy separation $\Delta\epsilon = \epsilon_{2,p} - \epsilon_{1,p} = (b_2 - b_1)k^2$ between the upper and lower states within each pair.

Accordingly, most significant deviations of the PT energies from the FT energies occur close to the $\bar{\Gamma}$ point and the size of this region in the BZ scales as $\sqrt{\xi}$. In particular, the energies $\epsilon_{j,p}^{\text{PT},\perp}$ diverge at $k = 0$ (where $\Delta\epsilon = 0$) while the exact energies $\epsilon_{j,p}^{\text{FT},\perp}$ remain finite [cf. Eq. (22)]. This large discrepancy between the FT and PT energies at small $k = |\mathbf{k}|$ arises because the standard PT formula [Eq. (23)] fails if the difference $\Delta\epsilon$ between the unperturbed energies $\epsilon_{2,p}$ and $\epsilon_{1,p}$ is substantially smaller than the module $|V| = \frac{1}{2}\xi$ of the perturbation matrix element. In this case, the PT formulation for degenerate states should be applied, with the 2×2 Hamiltonian matrix being initially diagonalized. This, in fact, would reproduce the exact (FT) result because all perturbation terms vanish as the SOC does not couple states from different pairs of QW states. Effective application of the degenerate PT to the entire system of the Co film is also not possible due to the presence of numerous closely spaced quantum states, as seen in Figs. 9 and 10. This would require prior diagonalization of the full Hamiltonian matrix, as in the FT approach. In consequence, the pragmatic PT approach to the calculations of the MCA energy involves the use of the second-order non-degenerate PT. This method has demonstrated good accuracy at moderate strengths of the SOC [4, 5, 21–23, 31, 35], despite its limitations for individual electron energies. However, as discussed in Sec. III A, this standard PT approach can lead to significantly inaccurate results for the MCA energy, particularly its oscillatory variation, at strong SOC.

2. Contributions to magnetocrystalline energy from quantum-well states. Force theorem versus perturbation theory

The discrepancy between the FT and PT results is now investigated by examining the contribution to the MCA energy from the model subsystem of the QW state pairs at various SOC strengths. The contribution at a specific wavevector \mathbf{k} is then defined in the FT approach as follows

$$E_{\text{MCA,QW}}^{\text{FT}}(\mathbf{k}) = \Omega_{\text{QW}}^{\text{FT},\perp}(\mathbf{k}) - \Omega_{\text{QW}}^{\text{FT},\parallel}(\mathbf{k}) \quad (24)$$

where the grand potential

$$\Omega_{\text{QW}}^{\text{FT},D}(\mathbf{k}) = \sum_p [g(\epsilon_{1,p}^{\text{FT},D}) + g(\epsilon_{2,p}^{\text{FT},D})] \quad (25)$$

is calculated with the energies $\epsilon_{j,p}^{\text{FT},D}$ of the perturbed QW state pairs for the two considered magnetization directions, out-of-plane ($D = \perp$) and in-plane ($D = \parallel$); see Eqs. (21) and (20). In the PT approach, the respective contribution to the MCA energy,

$$E_{\text{MCA,QW}}^{\text{PT}}(\mathbf{k}) = \frac{\xi^2}{4} \sum_p \frac{f_0(\epsilon_{2,p}) - f_0(\epsilon_{1,p})}{\epsilon_{2,p} - \epsilon_{1,p}}. \quad (26)$$

is given in terms of the energies $\epsilon_{j,p}$ and occupation factors $f_0(\epsilon_{j,p})$ in the unperturbed system.

The contributions to the MCA energy from the QW states around the $\bar{\Gamma}$ point are plotted along the $\bar{\Gamma} - \bar{X}$ line in Fig. 13. The k profiles of these contributions vary with the position $\epsilon_{0,\text{CP}}$ of the central pair of QW states at $k = 0$ relative to the Fermi level ($\epsilon_{\text{F0}} = 0$). This dependence is significant in the PT calculations, exhibiting a clear trend for any SOC, and for the SOC of Co and Pd (but not Pt) using the FT. The lowest profile is found for $\epsilon_{0,\text{CP}} = 0$, when the central pair contributes across the entire k range (down to $k = 0$). The highest profile occurs for $\epsilon_{0,\text{CP}} = \Delta\epsilon_0/2$ (or, equivalently, $\epsilon_{0,\text{CP}} = -\Delta\epsilon_0/2$), corresponding to the Fermi energy at the middle position $(\epsilon_{0,p-1} + \epsilon_{0,p})/2$ between the two neighbouring QW state pairs, as shown in Fig. 9(b). In this case, no pair contributes significantly in the interval of k near $k = 0$ where both states (lower and upper) of each pair lie either below or above the Fermi level. This interval constitutes a small region around the centre of the BZ ($0 \leq k < k_0$, e.g., $k \lesssim 0.12\pi/a_{2d}$ for $\Delta\epsilon_0 = 0.3$ eV, along the $\bar{\Gamma} - \bar{X}$ line). Within this region, the difference between the two profiles is most significant, being the largest at the $\bar{\Gamma}$ point ($k = 0$). The boundary of this region is located near the $k = k_0$ point where, for a subsystem of QW states with the central pair ($p = p_c$) at $\epsilon_{0,\text{CP}} = \Delta\epsilon_0/2$, the upper state from the neighbouring pair ($p = p_c - 1$, $\epsilon_{0,p} = -\Delta\epsilon_0/2$) crosses the Fermi level; see Fig. 13 (a,b). Indeed, for $k > k_0$, this latter pair gives a very similar contribution to the MCA energy as the central pair in a system with $\epsilon_{0,\text{CP}} = 0$. Accordingly, the region size k_0 is determined not by the SOC strength but by the spacing $\Delta\epsilon_0$ between the pairs of QW states and their k dispersion.

The full $\epsilon_{0,\text{CP}}$ dependencies of the QW state contributions at specific \mathbf{k} points are shown in Fig. 14. In both the FT

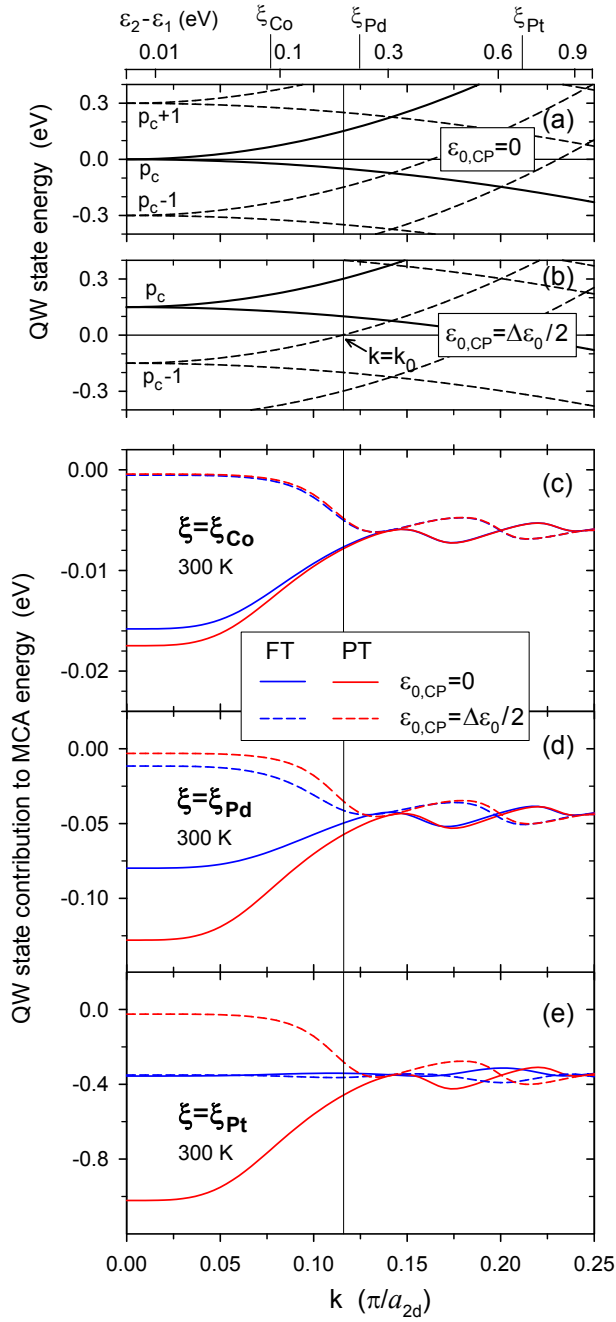


FIG. 13: (a,b) Energies of the model QW states in the Co film along the $\bar{\Gamma} - \bar{X}$ line near the BZ centre for (a) $\epsilon_{0,CP} = 0$ and (b) $\epsilon_{0,CP} = \Delta\epsilon_0/2$. (c-e) Contribution to the MCA energy from these states calculated using the FT (blue lines) and the PT (red lines) with the SOC constants (c) $\xi = \xi_{Co}$, (d) $\xi = \xi_{Pd}$, and (e) $\xi = \xi_{Pt}$ for $\epsilon_{0,CP} = 0$ (solid lines) and $\epsilon_{0,CP} = \Delta\epsilon_0/2$ (dashed lines) at $T = 300$ K, with $\Delta\epsilon_0 = 0.3$ eV and $\epsilon_F = \epsilon_{F0} = 0$. The top scale shows the energy separation $\Delta\epsilon = \epsilon_{2,p} - \epsilon_{1,p}$ in each pair of QW states, with the marked values of the SOC constants.

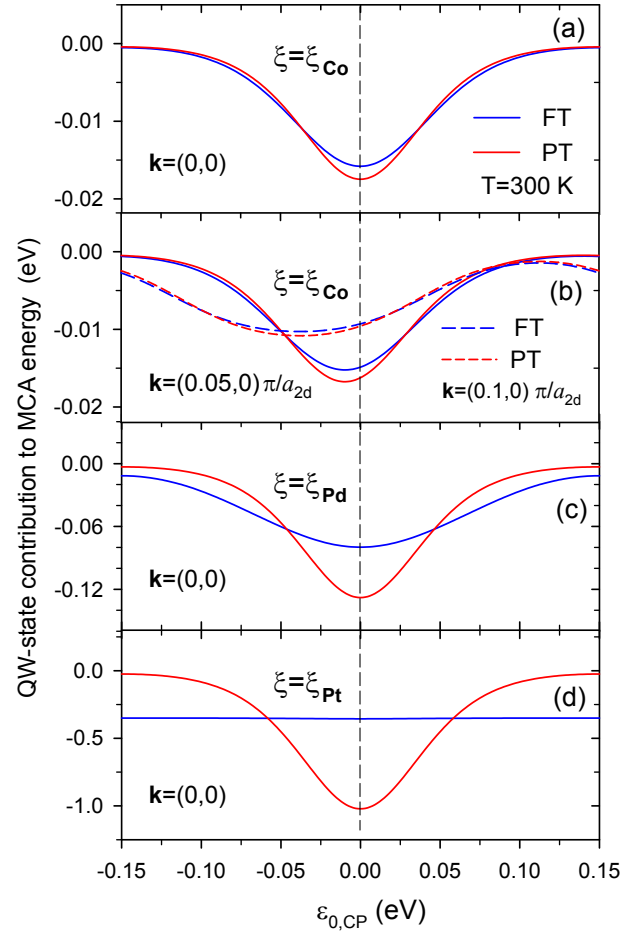


FIG. 14: (a-c) Contribution to the MCA energy from the model QW states at (a, c, d) $\mathbf{k} = (0,0)$, (b) $\mathbf{k} = (0.05,0)\pi/a_{2d}$ and (b) $\mathbf{k} = (0.1,0)\pi/a_{2d}$ in the Co film, calculated using the FT (blue line) and the PT (red line) versus the central QW state energy $\epsilon_{0,CP}$ (see Fig. 11). The results are obtained for the SOC constants of (a, b) $\xi = \xi_{Co}$, (b) $\xi = \xi_{Pd}$, and (c) $\xi = \xi_{Pt}$, with $\Delta\epsilon_0 = 0.3$ eV and $\epsilon_F = \epsilon_{F0} = 0$.

and PT approaches, the contributions calculated at $\mathbf{k} = (0,0)$ for the SOC strengths of Co and Pd, reach a negative minimum value for $\epsilon_{0,CP} = 0$ (at the Fermi level) and a maximum close to 0 for the energy $\epsilon_{0,CP} = \Delta\epsilon_0/2$. For non-zero \mathbf{k} near the $\bar{\Gamma}$ point, the positions of these minimum and maximum are slightly shifted to leftwards [to smaller $\epsilon_{0,CP}$; see Fig. 14(b)] which results from the asymmetric dispersion of the lower and upper bands in each QW state pair [$b_1 \neq -b_2$ in Eqs. (12) and (13)]. Note that the QW state contribution is the same for $\epsilon_{0,CP} = -\Delta\epsilon_0/2$ and $\epsilon_{0,CP} = \Delta\epsilon_0/2$ since the systems with such positions of $\epsilon_{0,CP}$ are equivalent.

These findings show that the simple model of QW states well captures the predictions of the FT and the PT for the MCA energy oscillations found for the full film system (Figs. 2, 7, and 8). The position of the central pair energy $\epsilon_{0,CP}$ changes by about $\Delta\epsilon_0/2$ when the Co thickness increases

from N_{Co} to $N_{\text{Co}}+1$ as illustrated for the films of Co(11 ML) and Co(12 ML) in Fig. 9. Thus, the $\epsilon_{0,\text{CP}}$ dependence of the QW state contribution explains the 2 ML period oscillations of the MCA energy (Figs. 1 and 4), which arise in the $\bar{\Gamma}$ region and have minima at $N_{\text{Co}} = 9, 11, 13$ ML and other thicknesses for which $\epsilon_{0,\text{CP}}$ is close to 0. The profiles of the model QW state contributions around the BZ centre, calculated using the FT and the PT for $\epsilon_{0,\text{CP}} = 0$ and $\epsilon_{0,\text{CP}} = \Delta\epsilon_0/2$, closely resemble the MCA energy distribution profiles obtained with the FT and PT for full film systems with similar positions of the central pair energy, such as the Co(11 ML) and Co(12 ML) films, respectively. The similarity between the full and QW state profiles of the MCA energy distributions holds not only for the moderate SOC of Co but also for the SOC of Pt; see Figs. 8 and 13(e).

The obtained k profiles of the QW state contribution also show that the discrepancy between the FT and PT distributions of the MCA energy close to the $\bar{\Gamma}$ point is clearly related to the inaccuracies of the PT energies of the QW states. The difference between the FT and PT profiles is most substantial in a k interval where these energies become inaccurate because the energy separation $\Delta\epsilon = (b_2 - b_1)k^2$ between the states in each pair is considerably smaller than the SOC constant ξ . The width of this interval is much smaller than $k_0 \approx 0.12\pi/a_{2d}$ for the nominal SOC of Co and grows with the SOC strength (as $\sqrt{\xi}$). It reaches k_0 for $\xi \sim \xi_{\text{Pd}}$ and exceeds k_0 for $\xi = \xi_{\text{Pt}}$. This is illustrated in Fig. 13, where the top scale shows $\Delta\epsilon$ and identifies the k points where $\Delta\epsilon$ is equal to ξ_{Co} , ξ_{Pd} , and ξ_{Pt} .

The relative difference between the PT and FT contributions also grows with the SOC strength. While the QW state contribution is still well described (even down to $k = 0$) by the PT for $\xi = \xi_{\text{Co}}$ at $T = 300$ K, the FT and PT profiles of this contribution largely differ for the SOC of Pd at the same temperature, though they still maintain similar shapes. For $\xi = \xi_{\text{Pt}}$, the PT completely fails to describe this contribution. Its k profiles and $\epsilon_{0,\text{CP}}$ dependence have the same shapes as for the weaker SOC (due to the ξ^2 scaling), which dramatically differs from the nearly flat k profiles and the extremely weak $\epsilon_{0,\text{CP}}$ dependence of the exact FT contribution; see Figs. 13(e) and 14(c). This explains why the FT distribution of the full MCA energy remains almost unchanged in the central part of the BZ when the film thickness is increased by 1 ML; see Fig. 8(a) and (c). Consequently, the oscillations of $E_{\text{MCA}}^{\text{FT}}(N_{\text{Co}})$ are many times smaller compared to the pronounced 2 ML oscillations predicted by the PT calculations [Fig. 8(b) and (d)].

In the model system, the change of the QW state contribution to the MCA energy upon increasing the Co thickness by 1 ML is given by the difference

$$A_{\text{MCA,QW}}^{\text{Y}}(\mathbf{k}, \epsilon_{0,\text{CP}}) = E_{\text{MCA,QW}}^{\text{Y}}(\mathbf{k})|_{\epsilon'_{0,\text{CP}}} - E_{\text{MCA,QW}}^{\text{Y}}(\mathbf{k})|_{\epsilon_{0,\text{CP}}} \quad (27)$$

(Y=FT, PT) between the values of this contribution for two positions of the central pair energy, $\epsilon_{0,\text{CP}}$ and $\epsilon'_{0,\text{CP}} = \epsilon_{0,\text{CP}} \pm \Delta\epsilon_0/2$, corresponding to Co thicknesses N_{Co} and $N_{\text{Co}} + 1$, respectively. This quantity represents the local amplitude

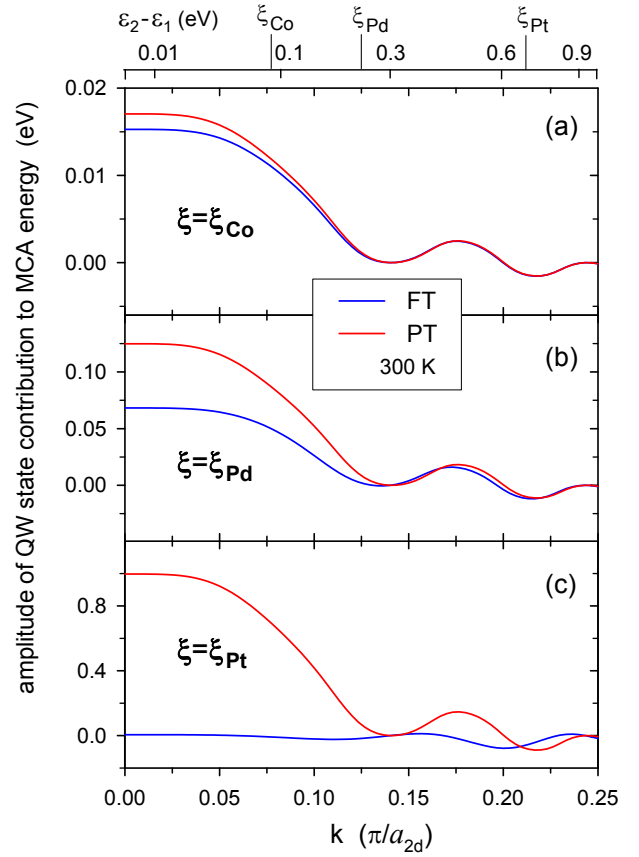


FIG. 15: Oscillation amplitude $A_{\text{MCA,QW}}^{\text{Y}}(\mathbf{k})$ (Y=FT, PT) [Eq. (27) with $\epsilon_{0,\text{CP}} = 0$] of the MCA energy contribution from the model QW states in the Co film along the $\bar{\Gamma} - \bar{X}$ line near the BZ centre. The amplitude is calculated using the FT (blue line) and the PT (red line) for (a) $\xi = \xi_{\text{Co}}$, (b) $\xi = \xi_{\text{Pd}}$, and (c) $\xi = \xi_{\text{Pt}}$, at $T = 300$ K, with $\Delta\epsilon_0 = 0.3$ eV. The top scale shows the energy separation $\Delta\epsilon = \epsilon_{2,p} - \epsilon_{1,p}$ in each pair of states, with the marked values of the SOC constants.

of the 2 ML period oscillations of the MCA energy due to QW states in the $\bar{\Gamma}$ region and can be either positive or negative. In the definition of $\epsilon'_{0,\text{CP}}$, the plus and minus signs are used for $\epsilon_{0,\text{CP}} < 0$ and $\epsilon_{0,\text{CP}} \geq 0$, respectively, so that both energies fall in the energy interval $[-\Delta\epsilon_0/2, \Delta\epsilon_0/2]$ relevant to central pairs. (alternatively, the plus sign could solely be used if this condition is relaxed and the periodicity in $\epsilon_{0,\text{CP}}$ is accounted for).

At the $\bar{\Gamma}$ point, the amplitudes $A_{\text{MCA,QW}}^{\text{FT}}$ and $A_{\text{MCA,QW}}^{\text{PT}}$ attain their maximum values for $\epsilon_{0,\text{CP}} = 0$ (with corresponding $\epsilon'_{0,\text{CP}} = \Delta\epsilon_0/2$) and vanish for $\epsilon_{0,\text{CP}} = -\Delta\epsilon_0/4$ (with $\epsilon'_{0,\text{CP}} = \Delta\epsilon_0/4$). This occurs because the contributions $E_{\text{MCA,QW}}^{\text{Y}}$ (Y=FT, PT) are symmetric functions of $\epsilon_{0,\text{CP}}$ at $\mathbf{k} = (0, 0)$; see Fig. 14. For \mathbf{k} points near the $\bar{\Gamma}$ point, the amplitude $A_{\text{MCA,QW}}^{\text{Y}}(\mathbf{k}, \epsilon_{0,\text{CP}})$ attains its maximum for a central pair energy slightly off the Fermi level ($\epsilon_{0,\text{CP}} \neq 0$). This behaviour results from the asymmetric $\epsilon_{0,\text{CP}}$ dependence of the $E_{\text{MCA,QW}}^{\text{Y}}$ (Y=FT, PT) contribu-

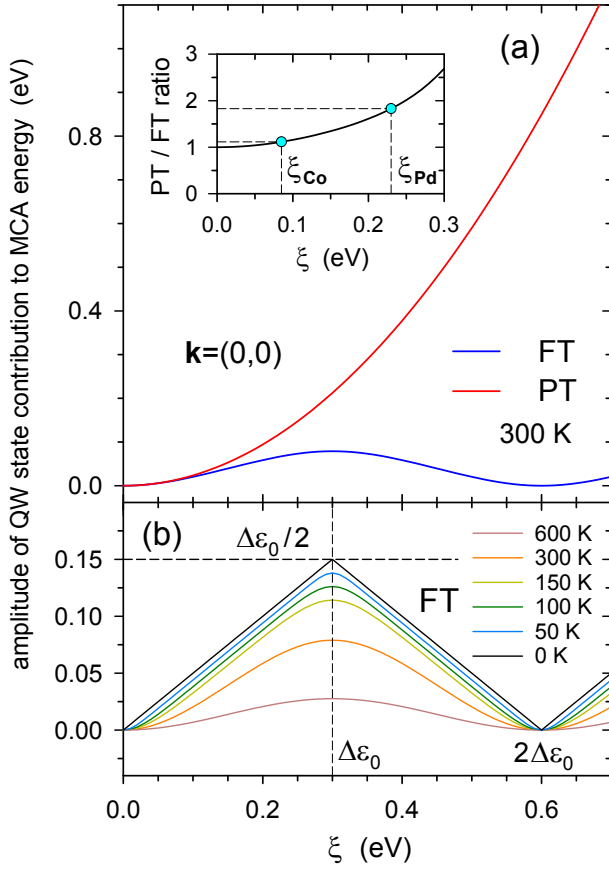


FIG. 16: (a,b) Oscillation amplitude $A_{\text{MCA,QW}}^Y(\mathbf{k})$ ($Y=\text{FT, PT}$) [Eq. (27) with $\epsilon_{0,\text{CP}} = 0$] of the MCA energy contribution from the model QW states at $\mathbf{k} = (0,0)$ in the Co film versus the SOC constant ξ . The amplitude is calculated with (a) the FT (blue line) and the PT (red line) at $T = 300$ K, and using (b) the FT at various temperatures, for the spacing of $\Delta\epsilon_0 = 0.3$ eV between QW state pairs (see Fig. 11). (a) Insert: PT to FT amplitude ratio versus ξ .

tion for $k > 0$ [see Fig. 14(b)], which is a direct consequence of the asymmetric dispersions ($b_1 \neq -b_2$) of the lower and upper bands in each QW state pair. Note that the central pair energy can be at various positions within the interval $-\Delta\epsilon_0/2 \leq \epsilon_{0,\text{CP}} \leq \Delta\epsilon_0/2$, depending on the Co film thickness. This is because the shifts of this energy with increasing N_{Co} are not exactly equal to $\pm\Delta\epsilon_0/2$ since the actual oscillation period of 2.12 ML of the MCA energy slightly differs from 2 ML [38]. This leads to oscillations of E_{MCA} with a modulated amplitude, similar to a beating pattern, with a modulation period of approximately 17 ML ($\approx 2/0.12$ ML), such as seen in Figs. 1 and 4.

The oscillation amplitudes $A_{\text{MCA,QW}}^{\text{FT}}(\mathbf{k})$ (for $\xi = \xi_{\text{Co}}$ and ξ_{Pd}) and $A_{\text{MCA,QW}}^{\text{PT}}(\mathbf{k})$ (for all ξ), calculated with $\epsilon_{0,\text{CP}} = 0$, are sizable in the interval $0 \leq k \lesssim k_0 \approx 0.12\pi/a_{2d}$ (for $\Delta\epsilon_0 = 0.3$ eV) and largest at the $\bar{\Gamma}$ point; see Fig. 15. For ξ less than 0.1 eV, the amplitudes obtained with the FT and the PT are very similar, differing less than 16%

at $\mathbf{k} = (0,0)$; see Fig. 16. However, the difference between these amplitudes increases rapidly with increasing ξ . For the SOC of Pd ($\xi = 0.23$ eV), the PT amplitude at $\mathbf{k} = (0,0)$ is nearly twice as large as the FT amplitude. For stronger SOC, the discrepancy between the FT and PT predictions becomes even more pronounced, with the PT oscillation amplitude being several, or even tens, times larger than the corresponding amplitude obtained with the FT. This explains the presence of similar discrepancies between the amplitudes of the 2 ML period oscillations of the MCA energy obtained with the FT and PT for the full Co film with enhanced SOC (Fig. 2).

The (maximum) amplitude of the oscillatory term in the total MCA energy due to the considered QW states can be estimated by integrating $A_{\text{MCA,QW}}^Y(\mathbf{k})$ ($Y=\text{FT and PT}$) for $\epsilon_{0,\text{CP}} = 0$ over of the BZ region with $0 \leq k \leq k_L$ where $k_L = 0.5\pi/a_{2d}$, which covers most of the $\bar{\Gamma}$ region (very similar results are obtained for a smaller region with $k_L = k_0 = 0.12\pi/a_{2d}$ where the integrated amplitude is most substantial). For the sake of simplicity, the parameters b_1 and b_2 which define the dispersion of the QW states [Eqs. (12) and (13)] are assumed to be constant, by taking their respective averages over different \mathbf{k} directions. Then, the integral that defines the size of the oscillatory MCA term is approximated as follows

$$A_{\text{MCA,QW}}^Y = \frac{2\pi}{\Omega_{\text{BZ}}} \int_0^{k_L} A_{\text{MCA,QW}}^Y(k) k dk \quad (28)$$

($Y=\text{FT and PT}$), with the normalized factor given by the inverse of the BZ volume Ω_{BZ} ; cf. Eq. (4). The so-estimated amplitude of the MCA energy oscillations at $T = 300$ K (Fig. 17) agrees well with the exact results for the MCA energy of the Co film with enhanced SOC (Fig. 2). In particular, the oscillation amplitudes have similar magnitudes in the calculations for the full film and the QW state model, in both FT and PT approaches. Notably, the PT amplitudes are much larger than the FT amplitudes, except for the film with the nominal Co SOC strength where the two amplitudes are nearly equal at $T = 300$ K. The model also correctly reproduces the temperature dependence (Fig. 18), with the PT amplitudes substantially increasing with lowering the temperature, in contrast to much weaker temperature dependence of the FT amplitudes (Fig. 1).

Figure 18 also shows how the integrated amplitudes $A_{\text{MCA,QW}}^{\text{FT}}$ and $A_{\text{MCA,QW}}^{\text{PT}}$ change with the central pair energy $\epsilon_{0,\text{CP}}$ used to define $A_{\text{MCA,QW}}^Y(\mathbf{k})$ ($Y=\text{FT, PT}$) in Eq. (27). The maxima of these amplitudes are slightly shifted from the Fermi level ($\epsilon_{F0} = 0$, $\epsilon_F = 0$), towards negative $\epsilon_{0,\text{CP}}$, with smaller shifts for lower T . These shifts result from the aforementioned fact that the amplitude $A_{\text{MCA,QW}}^Y(\mathbf{k})$ attains its maximum at $\epsilon_{0,\text{CP}} = 0$ only for $\mathbf{k} = (0,0)$ while the position of this maximum is shifted to finite $\epsilon_{0,\text{CP}}$ for $\mathbf{k} \neq (0,0)$ as the dispersions of the QW states are not symmetric ($b_1 \neq -b_2$). With $\epsilon_{0,\text{CP}}$ values of 0.0335 eV for Co(9 ML), 0.0118 eV for Co(11 ML), -0.0053 eV for Co(13 ML), and -0.0180 eV for Co(15 ML) (marked on Fig. 18), the model predicts the largest oscillation amplitude $A_{\text{MCA,QW}}^{\text{PT}}$, with the strongest temperature dependence,

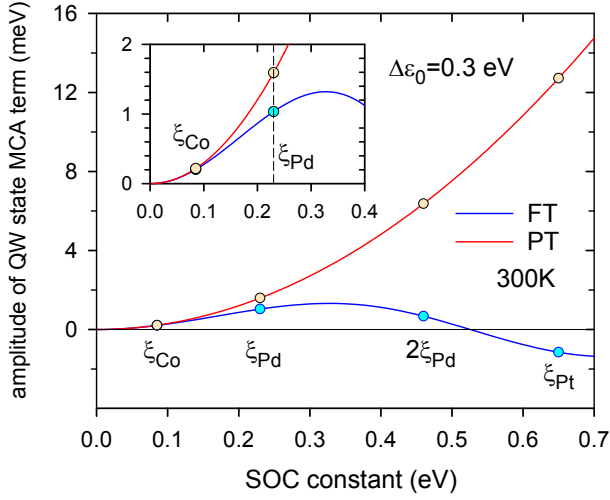


FIG. 17: Oscillation amplitude $\mathcal{A}_{\text{MCA,QW}}^Y(\mathbf{k})$ ($Y=\text{FT, PT}$) [Eqs. (28) and (27) with $\epsilon_{0,\text{CP}} = 0$] of the MCA energy term from the model QW states with $k \leq 0.5\pi/a_{2d}$ in the Co film versus the SOC constant ξ . The amplitude is calculated using the FT (blue line) and the PT (red line) at $T = 300$ K, with $\Delta\epsilon_0 = 0.3$ eV. Insert: Close-up of the main plot.

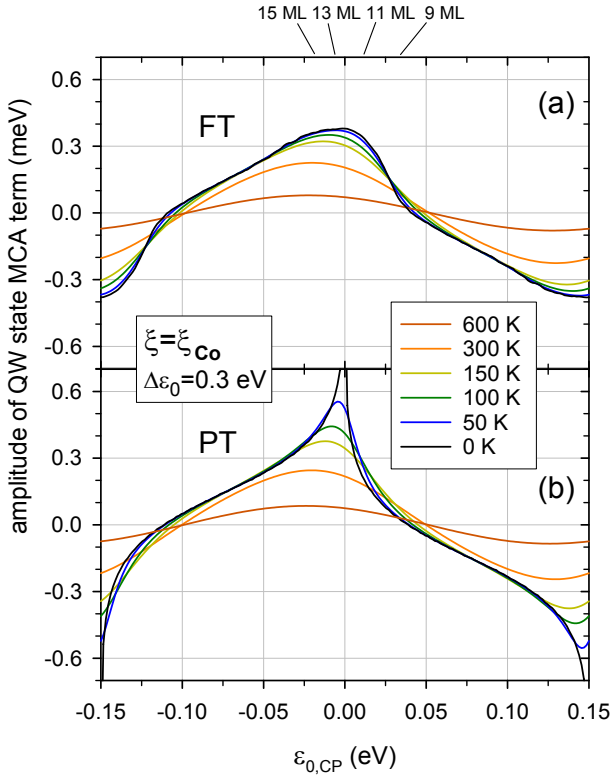


FIG. 18: Oscillation amplitude $\mathcal{A}_{\text{MCA,QW}}^Y$ ($Y=\text{FT, PT}$) of the MCA energy term [Eq. (28)] from the model QW states with $k \leq 0.5\pi/a_{2d}$ in the Co film with the nominal SOC ($\xi = \xi_{\text{Co}}$) versus the central pair energy $\epsilon_{0,\text{CP}}$. The amplitude is calculated using (a) the FT and (b) the PT at various temperatures, with $\Delta\epsilon_0 = 0.3$ eV. The values of $\epsilon_{0,\text{CP}}$ for selected Co films are marked on the top scale.

for the Co(13) film. This is in perfect agreement with the PT calculations for the full Co film system (Fig. 1). For larger values of $\epsilon_{0,\text{CP}}$, both negative and positive, the oscillation amplitude of the QW state term decreases and finally reverses its sign which corresponds to a change of the oscillation phase in the thickness dependence.

The model calculations show that at weak and moderate SOC (such as that of Co) and sufficiently high temperatures, the PT reproduces surprisingly well the predictions of the FT for the QW state contributions to the MCA energy even at very small k , where it fails for the energies of the perturbed QW states. To explain this apparent contradiction the QW state contribution at $k = 0$ (the $\bar{\Gamma}$ point) is expanded in a power series of ξ . This expansion is done by noting that the energies $\epsilon_{1,p}^{\text{FT},D}$ and $\epsilon_{2,p}^{\text{FT},D}$ at this point are equal to $\epsilon_{0,p} - \frac{1}{2}\xi$ and $\epsilon_{0,p} + \frac{1}{2}\xi$, respectively, for the out-of-plane magnetization ($D = \perp$) and $\epsilon_{0,p}$ for its in-plane direction ($D = \parallel$). The zeroth and odd-order terms in $E_{\text{MCA,QW}}^{\text{FT}}(k = 0)$, Eq. (24), cancel out, while the second-order term, given by the sum of $\frac{1}{4}f'(\epsilon_{0,p})\xi^2$ over p , reproduces the PT result [Eq. (26)] at $k = 0$ where the energies $\epsilon_{1,p}$ and $\epsilon_{2,p}$ are equal to $\epsilon_{0,p}$. The dominating term $\frac{1}{4}f'(\epsilon_{0,\text{CP}})\xi^2$ in this expansion comes from the central QW state pair, the one with $\epsilon_{0,p}$ closest to the Fermi energy. The fourth-order term $\frac{1}{96}f'''(\epsilon_{0,\text{CP}})\xi^4$, associated with this pair, can serve as an estimate of the error in the second-order PT expression for $E_{\text{MCA,QW}}^{\text{PT}}(k = 0)$, resulting from the neglect of higher-order terms. For $\epsilon_{0,\text{CP}} = 0$ at the Fermi energy, the fourth-order term is positive and is the following fraction of the second-order term

$$R_{4/2} = -\frac{1}{96} \left(\frac{\xi}{k_{\text{BT}}} \right)^2 \approx -\left(\frac{\xi}{10k_{\text{BT}}} \right)^2, \quad (29)$$

which depends on the ratio of the SOC constant ξ to k_{BT} . In particular, for $\xi = 0.085$ eV and $T = 300$ K ($k_{\text{BT}} = 0.02587$ eV), we obtain $R_{4/2} = -0.1125$ which elucidates why the PT is sufficiently accurate for the Co film with the nominal SOC at this temperature [see Fig. 13(c)]. However, for the SOC of Pd ($\xi = 0.23$ eV), the ratio $R_{4/2}$ reaches the value of -0.8234 at $T = 300$ K. This indicates, in agreement with the numerical results (Figs. 15 and 16), that the second-order PT provides only a rough approximation to $E_{\text{MCA,QW}}^{\text{PT}}(k = 0)$ for this SOC strength, and higher-order terms would be needed for an accurate description of the QW state contribution to the MCA energy. Note that the negative second-order term predicted by the PT is partially compensated by the positive fourth-order term, which results in a reduction of the oscillation amplitude. This is consistent with the numerical results which show a smaller amplitude of the MCA energy when calculated with the FT compared to the second-order PT, for both the QW state subsystem (Fig. 15) and the entire film (Fig. 2), with $\xi = \xi_{\text{Co}}$ and $\xi = \xi_{\text{Pd}}$. For the strongest considered SOC, $\xi = \xi_{\text{Pt}} = 0.65$ eV, the ratio of $R_{4/2}$ takes a huge value of -6.5760 which demonstrates that the PT formula is completely inadequate to describe the considered QW state contribution to the MCA energy. This explains why the PT so inaccurately predicts the thickness depen-

dence of the MCA energy in the Co film with the SOC of Pt [Fig. 2(d)].

The ratio $R_{4/2}$ increases with decreasing temperature which indicates that, in the PT approach, contributions from QW state pairs with energies very close to the Fermi level at $\mathbf{k} = (0, 0)$ become less accurate at lower T . This effect of decreasing temperature is reflected in the growing difference between the FT and PT results for the amplitude $\mathcal{A}_{\text{MCA,QW}}^Y$ ($Y=\text{FT, PT}$) of oscillations arising from the QW state subsystem with $\epsilon_{0,\text{CP}} \approx 0$ (Fig. 18). Such a trend is also found for the MCA energy of the full Co film system, in particular, at thicknesses of 13 and 15 ML (Fig. 1). For $\epsilon_{0,\text{CP}} = 0$, the contribution $E_{\text{MCA,QW}}^{\text{PT}}(k=0)$ diverges as $1/T$, leading to a divergent oscillation amplitude $\mathcal{A}_{\text{MCA,QW}}^{\text{PT}}$ at zero temperature. However, the oscillation amplitude is finite even at $T = 0$ because, for the actual Co films, the energy $\epsilon_{0,\text{CP}}$ never lies exactly at the Fermi level. Instead, it takes small, non-zero values, as reported above.

In the FT approach, the oscillation amplitude of the contribution $E_{\text{MCA,QW}}^{\text{FT}}(\mathbf{k})$ also increases with decreasing T for any ξ , but, unlike in the PT calculations, remains finite even in the $T = 0$ limit. This is illustrated for $k = 0$ in Fig. 16 (b). Consequently, the temperature dependence of the MCA energy (especially its oscillations) calculated with the FT is substantially weaker than that in the PT calculations, as seen for the Co film with the nominal SOC in Fig. 1 and previously reported for the Co/Pd bilayer in Ref. 23 (Fig. 10 therein). The amplitude $\mathcal{A}_{\text{MCA,QW}}^{\text{FT}}(k=0)$ reaches the maximum at $\xi = \Delta\epsilon_0$ and vanishes for $\xi = 0$ and $\xi = 2\Delta\epsilon_0$, which is reflected by a triangular ξ dependence at $T = 0$. Thus, the oscillation amplitude decreases with ξ for $\xi > \Delta\epsilon_0$ which further explains the large discrepancy between the PT and FT predictions for stronger SOC. Note that the value of $\xi = 2\Delta\epsilon_0$ is equal to 0.6 eV for the assumed interpair spacing $\Delta\epsilon_0 = 0.3$ eV (corresponding to $N_{\text{Co}} \approx 12$ ML) and it is close to the SOC of Pt ($\xi = 0.65$ eV).

To understand such a non-monotonic ξ dependence of the FT amplitude let us note that the energies of the p -th pair at $k = 0$ for the SOC constant ξ ,

$$\epsilon_{1,p}^{\text{FT},\perp} = \epsilon_{0,p} - \xi/2, \quad (30)$$

$$\epsilon_{2,p}^{\text{FT},\perp} = \epsilon_{0,p} + \xi/2, \quad (31)$$

are equal to the energies of the neighbouring pairs,

$$\epsilon_{2,p-1}^{\text{FT},\perp} = \epsilon_{0,p-1} + \xi'/2, \quad (32)$$

$$\epsilon_{1,p+1}^{\text{FT},\perp} = \epsilon_{0,p+1} - \xi'/2, \quad (33)$$

respectively, calculated with the SOC constant of $\xi' = 2\Delta\epsilon_0 - \xi$. Thus, when the contributions from all the QW states are summed up in Eqs. (24), (25), the oscillation amplitude of the resultant MCA energy contribution $E_{\text{MCA,QW}}^{\text{FT}}(k=0)$ is the same for the SOC strengths of ξ and $\xi' = 2\Delta\epsilon_0 - \xi$, if very tiny contributions to this amplitude from the end QW state pairs, which lie well below ($p = 1$) or well above ($p = P$) the Fermi level, are neglected. Then, the amplitude $\mathcal{A}_{\text{MCA,QW}}^{\text{FT}}(k=0)$, as a function of ξ , is symmetric about the point $\xi = \Delta\epsilon_0/2$, as shown in Fig. 16(b).

The FT results for the QW state contribution $E_{\text{MCA,QW}}^{\text{FT}}$ are obtained using Eq. (25), which incorporates the Fermi energy ϵ_F in the presence of the SOC via the $g(\epsilon)$ function. So far, for simplicity, the same Fermi energy, $\epsilon_F = \epsilon_{F0} = 0$, has been assumed in the FT and PT calculations for the QW state subsystem. However, in an actual Co film with a finite SOC, the Fermi energy is shifted slightly with respect to ϵ_{F0} , such that $\epsilon_F = \epsilon_{F0} + \Delta\epsilon_F$. The shift $\Delta\epsilon_F$ results from the changes of all electron energies within the film due to the SOC, so it is treated as an external parameter in the model of the QW state subsystem. In the FT calculations, the MCA energy contribution [Eq. (24)], expressed with the grand potential of this subsystem [Eq. (25)], effectively depends on the position of the central pair with respect to the Fermi level, $\epsilon_{0,\text{CP}} - \epsilon_F$ (alongside the interpair energy spacing $\Delta\epsilon_0$, the k dispersion parameters b_1, b_2 and the SOC coupling constant ξ). Thus, the change of the Fermi energy by $\Delta\epsilon_F$ is equivalent to calculating the QW state contribution at $\epsilon_{0,\text{CP}} - \Delta\epsilon_F$ (instead of $\epsilon_{0,\text{CP}}$) while keeping ϵ_F fixed at $\epsilon_{F0} = 0$. As a direct result, the profile of $E_{\text{MCA,QW}}^{\text{FT}}(k=0)$ determined as a function of $\epsilon_{0,\text{CP}}$ for $\epsilon_F = 0$ (Fig. 14) is shifted rightwards by $\Delta\epsilon_F$ when the Fermi energy is $\epsilon_F = \epsilon_{F0} + \Delta\epsilon_F$. This shift, in turn, moves the profile minimum from $\epsilon_{0,\text{CP}} = 0$ to $\epsilon_{0,\text{CP}} = \Delta\epsilon_F$.

For a Co film with $N_{\text{Co}} = 12$ ML, the Fermi energy shift $\Delta\epsilon_F = \epsilon_F - \epsilon_{F0}$ is small for the nominal SOC of Co(0.0041 eV) but increases significantly with stronger SOC, reaching 0.0271 eV for $\xi = \xi_{\text{Pd}}$, 0.0980 eV for $\xi = 2\xi_{\text{Pd}}$, and 0.180 eV for $\xi = \xi_{\text{Pt}}$. These shifts change only slightly for thicker Co films. Notably, the shifts $\Delta\epsilon_F$ are well approximated by the ξ^2 dependence predicted by the PT [23] across the whole considered SOC range. This indicates that the Fermi energy is less sensitive than the MCA energy to inaccuracies of the PT description at strong SOC perturbations.

However, the shift of the Fermi energy is irrelevant if we are primarily interested in the oscillation amplitude of the QW state contribution to the MCA energy, and comparing it between the FT and the PT. The amplitude $\mathcal{A}_{\text{MCA,QW}}^{\text{FT}}(\mathbf{k})$ is invariant under such a shift since it corresponds to shifting the $\epsilon_{0,\text{CP}}$ profile of this contribution. Consequently, the oscillation amplitude can be equivalently calculated by assuming $\epsilon_F = \epsilon_{F0} = 0$ and using the same two values of the central pair energy, $\epsilon_{0,\text{CP}}$ and $\epsilon'_{0,\text{CP}} = \epsilon_{0,\text{CP}} \pm \Delta\epsilon_0/2$, as in the PT approach. In particular, the energies $\epsilon_{0,\text{CP}} = 0$ and $\epsilon'_{0,\text{CP}} = \Delta\epsilon_0/2$ can be used to determine the maximum amplitude at $\mathbf{k} = (0, 0)$. These assumptions were made in the FT calculations, the results of which are shown in Figs. 13-18.

C. Magnetocrystalline anisotropy in Co/Pt bilayer calculated with force theorem and perturbation theory

The PT also fails to accurately reproduce the MCA energy obtained with the FT for the Co/Pt bilayer, as reported in Ref. 22 for $T = 300$ K. The present results for other temperatures (Fig. 19) confirm this discrepancy, showing that

the MCA energy oscillations in this system have a different pattern and larger amplitude in the PT calculations compared to the exact FT results. This difference becomes more pronounced at low temperatures. The discrepancy between the FT and PT results is different in different regions of the BZ (Fig. 20) and most evident in the contribution to the MCA energy from the $\bar{\Gamma}$ region, as for the Co film with an enhanced SOC constant (Figs. 4-6). These findings are visualized by the respective distributions of the MCA energy in the BZ, with the PT contributions largest around the $\bar{\Gamma}$ point and the FT distribution strongly smoothed out; see Fig. 21. In both approaches, the oscillation amplitude is much larger in the contribution to $E_{\text{MCA}} = E_{\text{MCA}}^Y$ ($Y=\text{FT}$ and PT) from the $\bar{\Gamma}$ region than the \bar{M} region while the \bar{X} region contributes the least to the MCA energy oscillations. The oscillatory term from the \bar{M} region exhibits a clear period of 5 ML in both the FT and PT approaches, while oscillations of the 2 ML period dominate in the contribution from the $\bar{\Gamma}$ region, as for the Co film.

In the PT calculations, the oscillations come from all spin-pair terms $E_{\text{MCA}}^{\sigma\sigma'}$, with same and opposite spins σ and σ' (Fig. 22). Two largest oscillatory contributions from the $\bar{\Gamma}$ region originate from the spin-pair terms involving the minority-spin states, $E_{\text{MCA}}^{\downarrow\downarrow}$ and $E_{\text{MCA}}^{\downarrow\uparrow} + E_{\text{MCA}}^{\uparrow\downarrow} = 2E_{\text{MCA}}^{\downarrow\uparrow}$, with the clear 2 ML period and similar amplitudes. However, these contributions have opposite phases so that largely cancel out when they are summed. As a result, the net amplitude of the 2 ML period oscillations becomes much smaller, allowing weaker oscillatory terms, such as the $E_{\text{MCA}}^{\uparrow\uparrow}$ term with the 3 ML and 4 ML periods, to become also significant in the $\bar{\Gamma}$ region contribution to $E_{\text{MCA}}^{\text{PT}}$. These two longer periods come from the QW sp states which originate from the majority-spin band in bulk Co and cross the Fermi level ϵ_{F0} regularly as the Co layer thickness increases. Specifically, these states cross ϵ_{F0} with the period of 4.12 ML at $\mathbf{k} = (0,0)$ (the $\bar{\Gamma}$ point) [22], but the period reduces to approximately 3 ML at \mathbf{k} distant by $0.1k_{\text{D}}$ from the $\bar{\Gamma}$ point (where k_{D} is $|\bar{\Gamma}-\bar{M}|$). The diagonal spin-pair terms $E_{\text{MCA}}^{\downarrow\downarrow}$ and $E_{\text{MCA}}^{\uparrow\uparrow}$ include, apart from interband contributions, also intraband contributions [Eq. (7)], which partly cancel out oscillations of the former and arise due to the lack of the inversion symmetry in the Co/Pt bilayer.

The total intraband term of the MCA energy $E_{\text{MCA}}^{\text{PT}} = E_{\text{MCA, intra}} + E_{\text{MCA, inter}}$ is of comparable magnitude as its interband term and the two terms largely cancel out (see Fig. 19), as it was previously found for the Co/Pd and Co/Cu bilayers [22, 23]. The oscillations of $E_{\text{MCA, intra}}$ are smaller than those of $E_{\text{MCA, inter}}$ in most of the Co thickness range, especially at lower temperatures. However, the intraband term can substantially increase for specific Co/Pt films where one of nearly flat energy bands $\epsilon_{n\sigma}(\mathbf{k})$ in the vicinity of the $\bar{\Gamma}$ point lies almost exactly at the Fermi level, as for the Co(10 ML)/Pt(8 ML) bilayer; see Fig. 23(a). The intraband contribution $\frac{1}{2}f_0'(\epsilon_{n\sigma})[\epsilon_{n\sigma}^{(1)}]^2$ from such a band, proportional to $-\delta(\epsilon_{n\sigma} - \epsilon_{\text{F0}})$ at $T \rightarrow 0$, then leads to a strong peak in the $E_{\text{MCA}}^{\text{PT}}(N_{\text{Co}})$ variation (at $N_{\text{Co}} = 10$ ML in Fig. 19), in a similar way as peaks of the DOS arise.

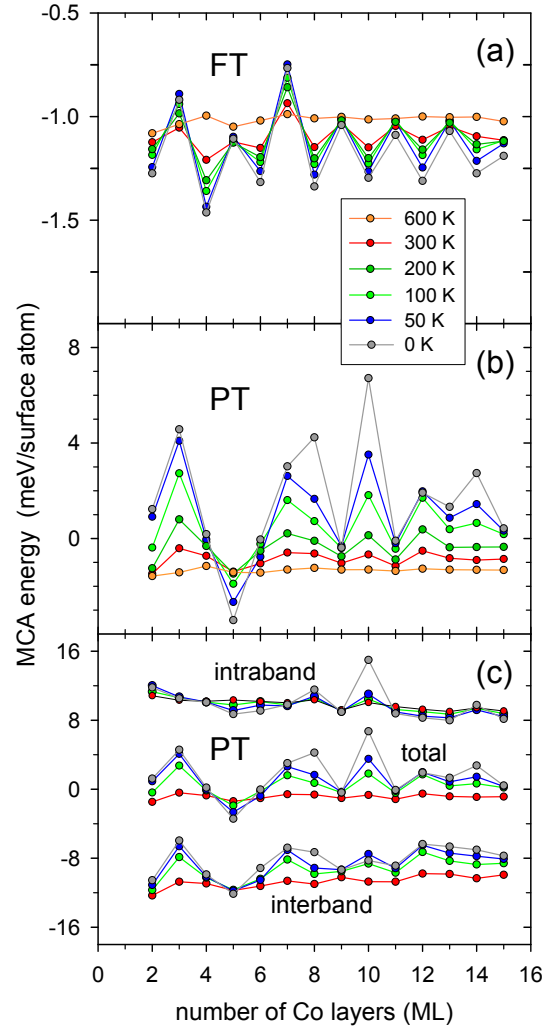


FIG. 19: MCA energy of the (001) fcc Co/Pt(8 ML) bilayer calculated with the (a) FT and (b,c) the PT at various temperatures. (c) Intraband and interband terms of $E_{\text{MCA}}^{\text{PT}}$.

These findings show that the origin of the MCA energy oscillations in the Co/Pt bilayer, as described by the PT, is more complex than in the Co film. Unlike the Co film, where only minority-spin state pairs contribute to these oscillations, the bilayer's oscillations arise from pairs of states with both same and opposite spins, as well as individual states which give intraband contributions. Furthermore, although these oscillations are induced by changes of the Co layer thickness, they do not arise primarily from the SOC within the Co part of the bilayer. In fact, the MCA energy and its oscillations in the Co/Pt bilayer arise almost entirely from the large SOC of the Pt layer, as it is demonstrated in Ref. 22 by decomposing the PT expression for the MCA energy into four terms $E_{\text{MCA}}^{\text{XY}}$, proportional to the products $\xi_X \xi_Y$ of the SOC constants, where X and Y are Co or Pt.

This scenario is possible because states in the Co layer near the Fermi energy hybridize with the d states in Pt layer, resulting in states that span over the whole bilayer, as pre-

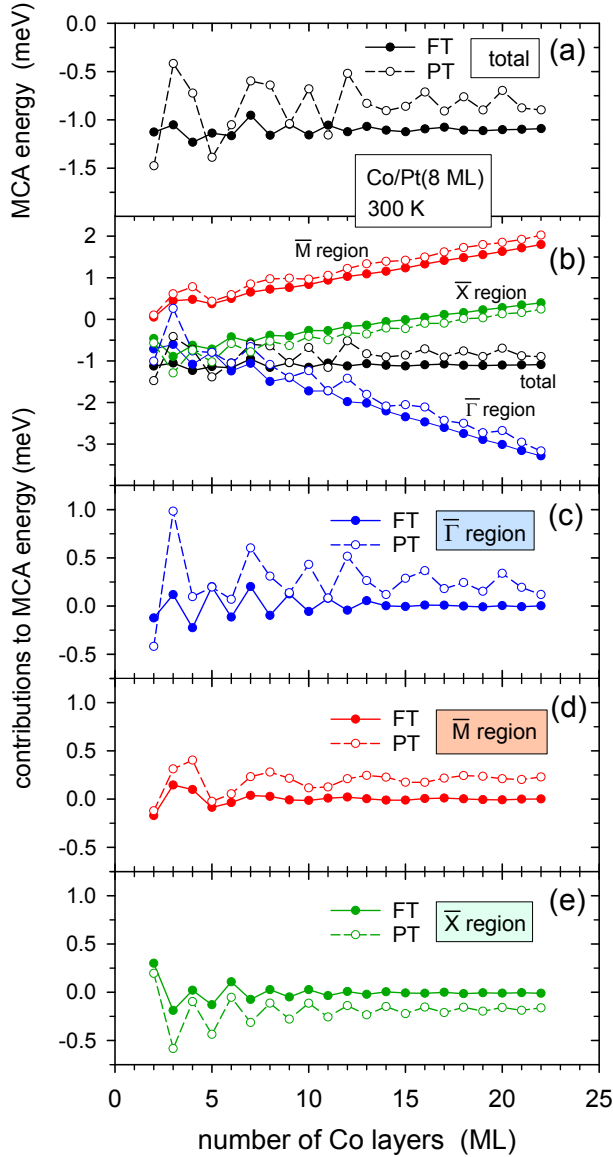


FIG. 20: (a) MCA energy calculated with the FT (solid circles) and the PT (open circles) for the (001) fcc Co/Pt(8 ML) bilayer at $T = 300$ K. (b) Contributions to this energy from different regions in the BZ (Fig. 3). (c-e) Oscillatory components of the MCA energy contributions from the (c) $\bar{\Gamma}$, (d) \bar{M} and (e) \bar{X} regions. Note: the same energy scale is used in panels (a,c-e).

viously found for similar delocalized states in the Pd/Co/Pd trilayer (Fig. 7 in Ref. 42) and the Co/Cu/Pt trilayer (Fig. 4 in Ref. 59)]. Such a hybridization occurs for both minority-spin d states and majority-spin sp states in Co, because d states of both spins are available near the Fermi level in the nonmagnetic Pt layer. Since the resultant states $|n\mathbf{k}\sigma\rangle$ have a finite probability in each layer [defined with their wavefunctions $\psi_{n\mathbf{k}\sigma}(\mathbf{r})$ as the spatial integral of $|\psi_{n\mathbf{k}\sigma}(\mathbf{r})|^2$ over the Co or Pt layer] the energies $\epsilon_{n\sigma}(\mathbf{k})$ of these states change as the thickness of the Co layer increases, providing a necessary condition for os-

cillations of the MCA energy enhanced by the SOC of Pt. The states with a significant probability in the Pt layer are subject to the large spin-orbit interaction in this layer and, thus, can strongly couple to other states of both spins that also have a substantial probability in the Pt layer. In particular, such coupling occurs within pairs of minority-spin states that span both Co and Pt layers, and are degenerate at the $\bar{\Gamma}$ point [$\mathbf{k} = (0, 0)$], as in the Co film. These states are predominantly composed of the yz and zx orbitals [or, more specifically, their two combinations, ϕ_1 and ϕ_2 , defined in Eq. (17)], but also contain minor components from other orbitals for $\mathbf{k} \neq (0, 0)$. Pairs of minority-spin states with such a spatial distribution and orbital composition are indeed present in the Co/Pt(8 ML) bilayer and have the probability of around $Q = 0.5$ in the Pt layer for the Co thicknesses of 10-12 ML (see Figs. 23 and 24). They contribute to the 2 ML period oscillations of the $E_{MCA}^{\downarrow\downarrow}$ term in the PT approach, with largest contributions coming from pairs with energies in the immediate vicinity of the Fermi level; see Fig. 25(a). Similar pairs of d states, predominately composed of the yz and zx orbitals and degenerate at the $\bar{\Gamma}$ point, also exist for majority spin and they are almost entirely confined within the Pt layer ($Q \approx 1$). Consequently, such majority-spin states near the Fermi level, as those seen in Figs. 24, can also strongly couple to the minority-spin QW states near the Fermi level [Fig. 25(b)], leading to the 2 ML period oscillations of the $E_{MCA}^{\downarrow\downarrow} + E_{MCA}^{\downarrow\uparrow} = 2E_{MCA}^{\downarrow\uparrow}$ term in the PT calculations (Fig. 22). Note that the oscillation amplitude of this term can be significantly reduced by substantial contributions from some other majority-spin states coupled to the minority-spin QW states, as shown in Fig. 25(b). Furthermore, the majority-spin states that are mostly localized in the Pt layer and arise from d states in Pt hybridized with sp states in Co contribute to oscillations of the MCA energy with longer periods of 3-4 ML. As already discussed, this contribution dominates in the $E_{MCA}^{\uparrow\uparrow}$ term, but it is also present, as a minor component, in the $E_{MCA}^{\downarrow\uparrow} + E_{MCA}^{\uparrow\downarrow}$ term. The described scenario is similar to the mechanism that underlies the experimentally observed MCA oscillations in the Co/Cu bilayer versus the Cu thickness, which are substantial despite a low DOS at the Fermi energy in Cu and primarily arise from the SOC in the Co layer [40]. In that system, the sp states in Cu hybridize with minority-spin d states in the Co film and the energies of the resultant states, mostly localized in the Co layer, shift and cross the Fermi level periodically as the Cu thickness increases.

States composed solely of yz , zx (which is strictly valid at the $\bar{\Gamma}$ point) are coupled only by the $L_z S_z$ terms of H_{so} , as discussed under Eq. (18). Thus, states with such an orbital composition and same spins can couple to each other only for out-plane magnetization (with spins along the easy axis $\zeta = z$) while the coupling between them vanishes for in-plane direction of magnetization ($\zeta = x$). The reverse is true for pairs of states with opposite spins where the finite coupling is present only for in-plane magnetization since the spin operator S_z is equivalent to $S_\eta = (S'_+ - S'_-)/2i$ in the rotated frame of reference $O\xi\eta\zeta$, with the ladder operators

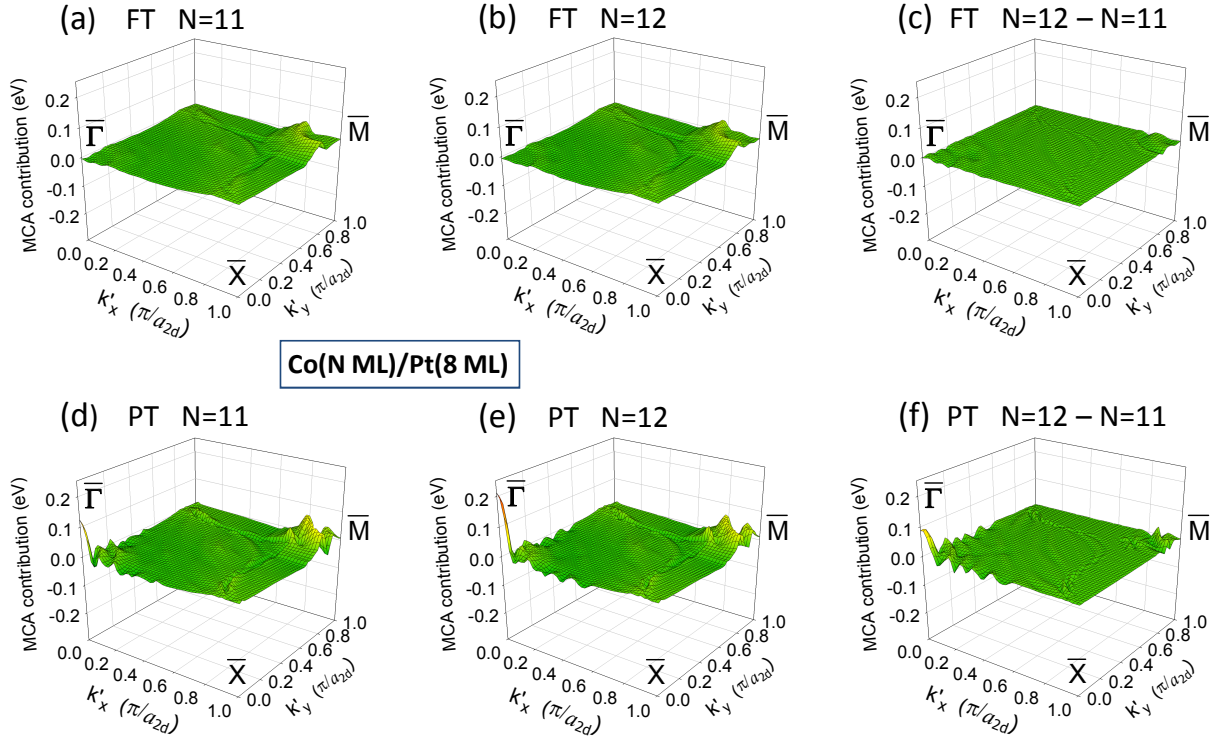


FIG. 21: Distribution of the MCA energy in the BZ for the (001) fcc (a,d) Co(11 ML)/Pd(8 ML) and (b,e) Co(12 ML)/Pd(8 ML) bilayers with $N = 11$ at $T = 300$ K, obtained with the FT (top row) and the PT (bottom row). (c,f) Difference between the 12 ML and 11 ML distributions. The plots show the symmetrized distributions (see Appendix A) in one quarter of the BZ.

S'_+ and S'_- acting on the spin states $|\downarrow\rangle$ and $|\uparrow\rangle$ quantized along the easy axis $\zeta = x$. Similar distinction, though less strict, with strong coupling for one magnetization direction and weak for the other, depending on the spins of the involved states, also holds in the vicinity of the $\bar{\Gamma}$ point where the considered QW states include minor components from other orbitals, in addition to yz and zx . As a result, contributions from pairs of such states with same and opposite spins come with opposite signs in the MCA energy $E_{\text{MCA}}^{\text{PT}} = \Omega^{(2)}(\hat{\mathbf{M}}_{\perp}) - \Omega^{(2)}(\hat{\mathbf{M}}_{\parallel})$. This explains why the 2 ML period oscillations of the spin-pair terms $E_{\text{MCA,inter}}^{\downarrow\downarrow}$ and $E_{\text{MCA}}^{\downarrow\uparrow} + E_{\text{MCA}}^{\uparrow\downarrow}$ are in antiphase and largely cancel out, which reduces the amplitude of the 2 ML period oscillations in the total MCA energy, as seen in Fig. 22. An additional reduction of its oscillation amplitude arises due to intraband contributions in $\Omega^{(2)}$ [Eq. (4)] which are non-zero only for in-plane magnetization so that the term $E_{\text{MCA,intra}}^{\downarrow\downarrow}$ also oscillates with the Co thickness in antiphase to the interband term $E_{\text{MCA,inter}}^{\downarrow\downarrow}$.

The cancellations of the oscillatory spin-pair terms in the PT approach lead to around three-fold reduction in the oscillation amplitude of the net MCA energy, compared to its $E_{\text{MCA,inter}}^{\downarrow\downarrow}$ term. However, this only partly explains why the amplitude of the MCA energy obtained with the PT for the CoPt bilayer is much smaller than that for the Co film with the SOC of Pt, where only the term $E_{\text{MCA}}^{\downarrow\downarrow} = E_{\text{MCA,inter}}^{\downarrow\downarrow}$ due

to minority-spin state pairs contributes to the oscillations of $E_{\text{MCA}}^{\text{PT}}$ (see Fig. 3 in Ref. [22]). Another reason for this difference is that the effective strength of the SOC in the CoPt bilayer is smaller than that of Pt. Indeed, minority-spin QW states $\psi_{n\mathbf{k}\downarrow}(\mathbf{r})$ that span over a Co/Pt bilayer can be formally represented, as sums of two states $\psi_{n\mathbf{k}\downarrow}^{\text{X}}(\mathbf{r})$, one confined in the X=Co layer and the other in the X=Pt layer,

$$\psi_{n\mathbf{k}\downarrow}(\mathbf{r}) = a\psi_{n\mathbf{k}\downarrow}^{\text{Co}}(\mathbf{r}) + b\psi_{n\mathbf{k}\downarrow}^{\text{Pt}}(\mathbf{r}), \quad (34)$$

with respective probability amplitudes a and b (where $|a|^2 + |b|^2 = 1$; note that a does not denote the lattice constant here). The effective SOC constant in the matrix elements $\langle n\mathbf{k}\downarrow | H_{\text{so}} | n'\mathbf{k}\downarrow \rangle$ entering the $E_{\text{MCA}}^{\downarrow\downarrow}$ term is then approximated as

$$\xi_{\text{eff}}^{\downarrow\downarrow} = |a|^2 \xi_{\text{Co}} + |b|^2 \xi_{\text{Pt}} \approx |b|^2 \xi_{\text{Pt}}, \quad (35)$$

given that ξ_{Pt} is nearly eight times larger than ξ_{Co} . With the probability in Pt of $Q = |b|^2 \approx 0.5$ for the QW states near the $\bar{\Gamma}$ point (Fig. 23), the value of $\xi_{\text{eff}}^{\downarrow\downarrow}$ is close to $\xi_{\text{Pt}}/2$ and their contribution to $E_{\text{MCA}}^{\downarrow\downarrow}$ is proportional to $(\xi_{\text{eff}}^{\downarrow\downarrow})^2 \approx 0.25\xi_{\text{Pt}}^2$. Majority-spin d states near the Fermi level $\psi_{n\mathbf{k}\uparrow}(\mathbf{r}) = \psi_{n\mathbf{k}\uparrow}^{\text{Pt}}(\mathbf{r})$, which are entirely confined within the Pt layer (Fig. 24), are subject to the SOC of Pt only. Accordingly, the contribution from pairs of QW states with opposite spins to $E_{\text{MCA}}^{\downarrow\uparrow}$ and $E_{\text{MCA}}^{\uparrow\downarrow}$ involves the factor $(\xi_{\text{eff}}^{\downarrow\uparrow})^2 = |b|^2 \xi_{\text{Pt}}^2$ which defines the respective effective

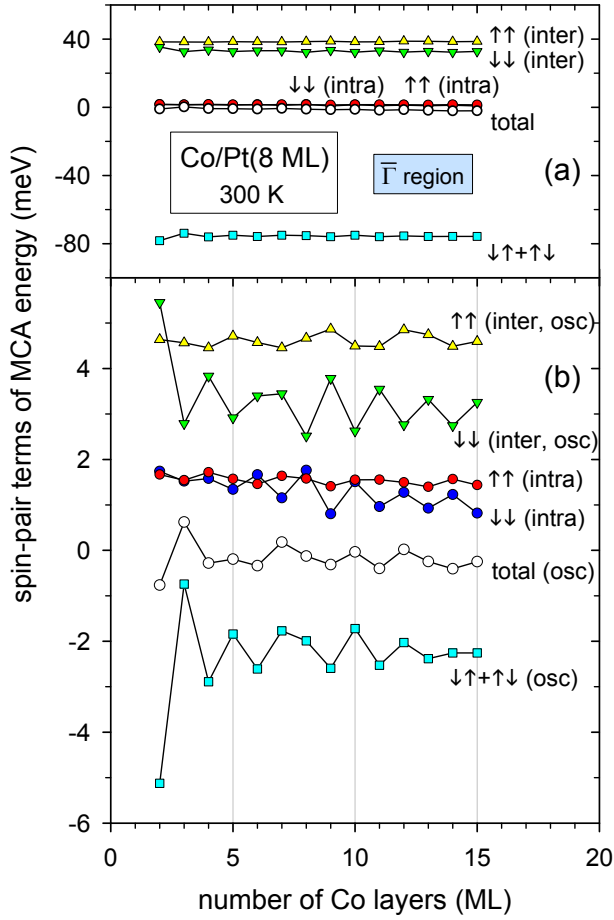


FIG. 22: (a) Spin-pair terms of the contribution to the MCA energy from the $\bar{\Gamma}$ region in the BZ calculated with the PT for the (001) fcc Co/Pt(8 ML) bilayer at $T = 300$ K. (b) Oscillatory parts of the spin-pair terms and the total $\bar{\Gamma}$ region contribution. The $\downarrow\downarrow$ and $\uparrow\uparrow$ terms are separated into their respective interband and intraband parts; see Eq. (7).

constant

$$\xi_{\text{eff}}^{\downarrow\uparrow} = |b|\xi_{\text{Pt}}, \quad (36)$$

close to $0.7\xi_{\text{Pt}}$ for $|b|^2 \approx 0.5$.

Thus, the reduced effective SOC in the Co/Pt bilayer helps to explain further why the discrepancy between the PT and FT predictions is smaller in this system compared to the standalone Co film with the full SOC of Pt (see Figs. 2(d) and 19). Another example that follows a similar rule is the Co/Pd bilayer for which the PT describes the MCA energy and its oscillations with good accuracy (at $T = 300$ K), while a larger discrepancy between the PT and FT is found for a Co film with the SOC of Pd; see Fig. 2(b) in Ref. 22 and Fig. 2(b) in this paper, respectively.

In the FT approach, the QW state contribution to the grand potential for out-of-plane magnetization can be approximately described using a simplified model of equidistant pairs of minority-spin QW states (strongly coupled for

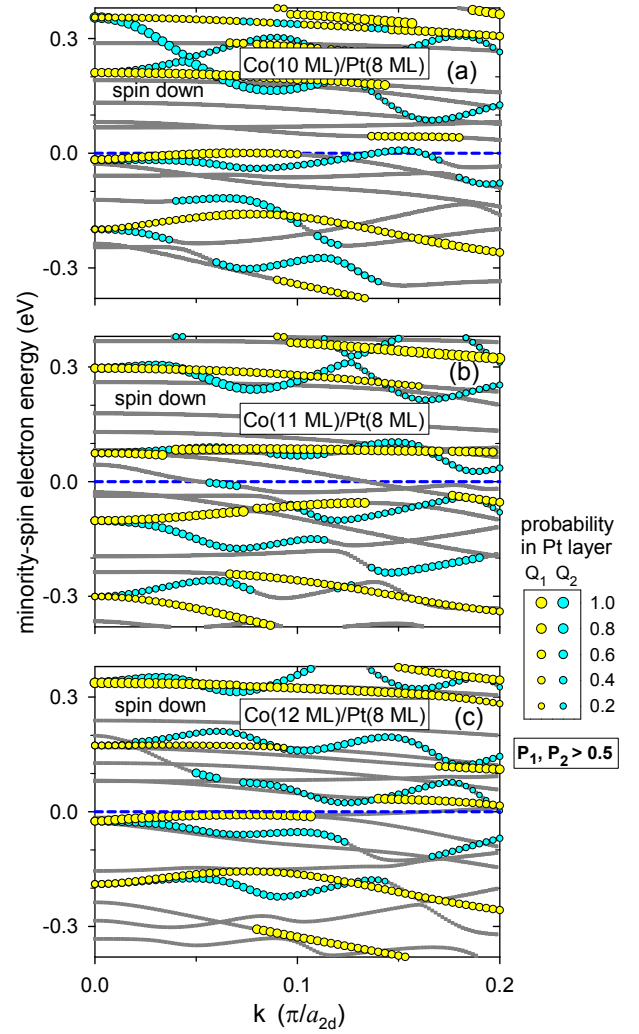


FIG. 23: (a,b,c) Minority-spin electron energies along the $\bar{\Gamma} - \bar{X}$ line for the (001) fcc (a) Co(10 ML)/Pt(8 ML), (b) Co(11 ML)/Pt(8 ML) and (c) Co(12 ML)/Pt(8 ML) bilayers without the SOC. The colour-marked bands indicate states with projections $P_1 \geq 0.5$ onto the $|\phi_1\rangle = (|yz\rangle - |zx\rangle)/\sqrt{2}$ orbital (yellow circles) and $P_2 \geq 0.5$ onto the $|\phi_2\rangle = (|yz\rangle + |zx\rangle)/\sqrt{2}$ orbital (light blue circles); P_1 and P_2 are equal to 1 at $k = 0$. The size of colour symbols is proportional to the total probabilities of these states in the Pt layer, Q_1 and Q_2 , respectively, according to the side scale. The Fermi energy is at $\epsilon_{F0} = 0$ (horizontal dashed line).

this magnetization direction), with the Hamiltonian decomposed into 2×2 blocks, as for the Co film. An extension of this model to the case of in-plane magnetization is not straightforward since it would also require including a subset of majority-spin states and diagonal (intraband) matrix elements $\langle n\mathbf{k}\sigma | H_{\text{so}} | n\mathbf{k}\sigma \rangle$ of the SOC operator. Although these elements vanish for the states $|n\mathbf{k}\sigma\rangle$ composed solely of yz and zx orbitals, for both magnetization directions, they are finite for in-plane magnetization in the vicinity of the $\bar{\Gamma}$ point, due to minor orbital components, the share

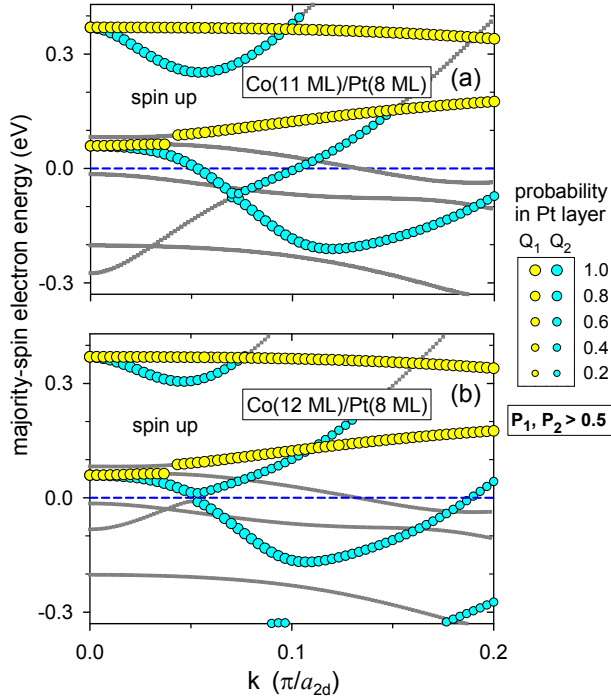


FIG. 24: (a,b) Majority-spin electron energies along the $\bar{\Gamma} - \bar{X}$ line for the (001) fcc (a) Co(11 ML)/Pt(8 ML) and (b) Co(12 ML)/Pt(8 ML) bilayers without the SOC. The colour-marked bands (yellow and light blue circles) are defined as in Fig. 23.

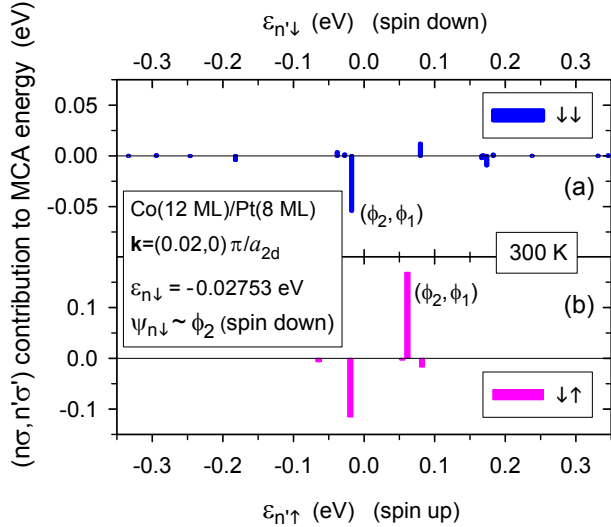


FIG. 25: (a,b) MCA energy contributions $E_{MCA}^{n\sigma, n'\sigma'}$ from selected pairs of electron states at $\mathbf{k} = (k'_x, k'_y) = (0.02, 0)\pi/a_{2d}$ in the Co(12 ML)/Pt(8 ML) bilayer at $T = 300$ K. The minority-spin state $|n\mathbf{k}\sigma\rangle$ ($\sigma = \downarrow$) (predominant $|\phi_2\rangle = (|yz\rangle + |zx\rangle)/\sqrt{2}$ orbital composition, $\epsilon_{n\downarrow} = -0.02753$ eV) is coupled to other states $|n'\mathbf{k}\sigma'\rangle$ of (a) minority ($\sigma' = \downarrow$) and (b) majority ($\sigma' = \uparrow$) spins. The two largest contributions from coupling to states with the predominant $|\phi_1\rangle = (|yz\rangle - |zx\rangle)/\sqrt{2}$ composition are marked.

of which cannot be easily estimated. Nevertheless, we can still expect that since, for each spin, the subset of unperturbed QW states can be approximately represented with a sequence of equidistant energies, the oscillation amplitude of the MCA energy determined within the FT approach is limited by the finite energy spacings between the consecutive QW states pairs, in a similar way as for the Co film with enhanced SOC where QW d states of minority-spin are present only; see Sec. III B 2. Such a plausible limitation may well explain why the oscillation amplitudes have similar magnitudes for the Co/Pd [22, 23] and Co/Pt bilayers in the FT approach, despite a large difference in the SOC strength between the two systems, while the oscillation amplitude is a few times larger for the Co/Pt bilayer in the PT calculations.

IV. CONCLUSIONS

The present work examines limitations of the PT in calculations of the MCA energy for layered systems with strong SOC and aims to reveal the origin of these limitations. The differences between the exact FT and approximate PT results are most evident in the oscillations of the MCA energy, with the PT calculations predicting a considerably larger oscillation amplitude while the average value is less affected. This discrepancy between the two approaches grows with increasing the SOC strength, whether it is the SOC of the nonmagnetic layer in the Co/Cu [23], Co/Pd [23] and Co/Pt bilayers or the enhanced SOC in the Co film. Substantial deviations of the PT predictions from the FT values of the MCA energy are also found for the Co film with the nominal SOC at low temperatures (100 K and lower), similar to previous findings on MCA energy oscillations in the Co/Pd bilayer [23].

The MCA energy calculated for the Co/Pt bilayer in the FT approach shows a moderate dependence on temperature, which defines smearing of energy levels. In contrast, this energy strongly depends on temperature in the PT calculations, with oscillation amplitude rapidly growing with decreasing temperature, down to $T = 0$. Consequently, the discrepancy between the FT and PT results for the Co/Pt bilayer becomes particularly pronounced at low temperatures. Such a temperature dependence of the MCA energy in systems with strong SOC can explain the largely differing values of this energy for the Fe(1ML)/Pt(1 ML) bilayers in the two separate PT calculations reported in Ref. 35. Namely, this difference can be attributed mainly not to the different *ab initio* codes applied, SIESTA [60] and VASP [61, 62], but rather the different values of the Fermi-Dirac smearing $k_B T$ assumed in these codes, 0.01 eV and 0.05 eV, respectively, which correspond to $T \approx 115$ K and $T \approx 580$ K. This also explains why the PT well reproduces the FT results using VASP, where the higher temperature is applied, while the discrepancy between the PT and FT values of the MCA energy is large for the lower temperature, used in SIESTA.

The PT contributions to the MCA energy deviate from its

FT distribution mostly near the high symmetry points where the oscillations due to respective QW states arise, with the largest deviations around the $\bar{\Gamma}$ point, and smaller, though still significant, deviations near the \bar{M} point. Accordingly, the results for the Co film with enhanced SOC are analyzed in depth using a simple model of minority-spin QW d states (composed of yz and zx orbitals) near the $\bar{\Gamma}$ point. The model provides an approximate description of the dominating 2 ML period oscillations of the MCA energy, showing good agreement with the numerical calculations for the full film system. It is shown that the discrepancy between the FT and PT predictions arises because the second-order PT formula (4) can fail to adequately describe contributions to the MCA energy from pairs of states with energy spacing smaller or comparable to the SOC strength. This is specifically the case for the considered pairs of QW states in the central region of the BZ which are doubly degenerate at the $\bar{\Gamma}$ point, and whose energies lie very close to the Fermi level at this point. For specific film thicknesses for which such a pair exists, the difference between the MCA energies obtained in the PT and FT calculations significantly grows with decreasing temperature, and the PT result even diverges at $T = 0$ when a pair energy lies exactly at the Fermi level at the $\bar{\Gamma}$ point. However, even in this case, the PT still reproduces the QW state contribution to the MCA energy with good accuracy when the SOC strength ξ is a few times smaller than $10k_B T$, as for the Co film with the nominal SOC at $T = 300$ K. Furthermore, the discrepancy between the FT and PT predictions for the MCA energy is much smaller and its temperature dependence is much weaker for film thicknesses for which no QW state pair is present in the immediate vicinity of the Fermi level, particularly when this level lies midway between two consecutive pairs at the $\bar{\Gamma}$ point. The determined dependence of the MCA energy oscillation amplitude on the energy of the central QW state pair (the one closest to the Fermi level) well explains how local oscillation amplitude changes with the Co film thickness.

Further, it is shown that, while the PT oscillation amplitude grows quadratically with increasing the SOC strength in the film, the FT amplitude follows this trend only for weak and moderate SOC (e.g., that of Co) and is limited by the finite energy spacing between the neighbouring QW state pairs when the SOC strength becomes comparable to this spacing. Consequently, the PT predicts a larger amplitude of the MCA energy oscillations than the exact FT approach, with particularly large difference for the Co film with the strong SOC of Pt. A similar limitation in the FT oscillation amplitude due to a sequence of QW state pairs is also expected for the Co/Pt bilayer where the amplitude predicted by the PT is a few times larger.

In the Co/Pt bilayer, the oscillations of the MCA energy with increasing thickness of the Co layer are mediated by the strong SOC in the Pt layer. Near the Fermi level, states of both spins in Co (minority-spin d states and majority-spin sp states) hybridize with d states in Pt and the MCA energy oscillations arise as the energies of the hybridized states change with the Co thickness. These states are cou-

pled by the SOC to other states of both spins, particularly strongly to those mostly localized in the Pt layer. As a result, the oscillations of the MCA energy calculated with the PT come from spin-pair terms with same (mainly minority) and opposite spins, which leads to large cancellations of 2 ML period oscillations and revealing weaker oscillations of longer periods in the thickness dependence of the MCA energy. In addition, the intraband terms which emerge due to the lack of the inversion symmetry in the Co/Pt bilayer also contribute to the MCA oscillations. In contrast, in the FT calculations, the oscillatory terms with longer periods play only a minor role in the oscillations of the MCA energy, which are dominated by the 2 ML period.

The states, which span over the whole Co/Pt bilayer, are subject to an effective SOC defined with a weighted average of the SOC constants of Co and Pt. Although the effective SOC constant is substantially reduced compared to that of Pt, it is still high enough to make the PT predictions for the MCA energy largely inaccurate, with oscillation amplitude 2-3 times greater than in the exact FT calculations. Since the states calculated in the presence of the SOC that are responsible for the MCA oscillations within the FT approach are also delocalized across the bilayer, their contributions to the MCA energy are also expected to reflect an effective, reduced SOC.

Although this work focuses on the effect of SOC on the MCA energy oscillations, it is also relevant to the total MCA energy. While average MCA energies calculated with the FT and PT show only moderate discrepancies at strong SOC, the MCA energy for a system with a specific thickness can exhibit significant discrepancies due to large differences between the oscillations of this energy predicted by the two approaches. Thus, the PT approach should be used with caution when examining the MCA energy (e.g., its spatial distribution [26, 27, 32]) in layered systems comprising elements with strong SOC. Accordingly, prior verification of agreement between FT and PT total MCA energies is crucial for a reliable application of PT results in further analysis.

Appendix A: Symmetrization of MCA energy distribution in Brillouin zone

The distribution of the MCA energy in the BZ, as defined with Eqs. (1) and (3), lacks the full symmetry of the system without the SOC, as shown in Figs. 26 (a) and (c). This is due to the reduced symmetry of the grand potential distribution in the presence of the SOC for in-plane magnetization, in particular, \mathbf{M} along the x axis. However, the symmetric distribution can be recovered by averaging (summing and dividing by eight) the contributions to $E_{\text{MCA}} = E_{\text{MCA}}^Y$ ($Y=\text{FT}$ and PT) over the star of each point $\mathbf{k} = (k_x, k_y)$, which comprises the eight equivalent points \mathbf{k}_i ($i = 1, 2, \dots, 8$) defined as $(\pm k_x, \pm k_y)$ or $(\pm k_y, \pm k_x)$ and generated by the respective symmetry operations \mathcal{R}_i .

Since the unperturbed energies $\epsilon_{n\sigma}$ are equal at all points \mathbf{k}_i , symmetrizing the distribution of the MCA energy defined in Eq. (4) within the PT framework amounts to averaging of

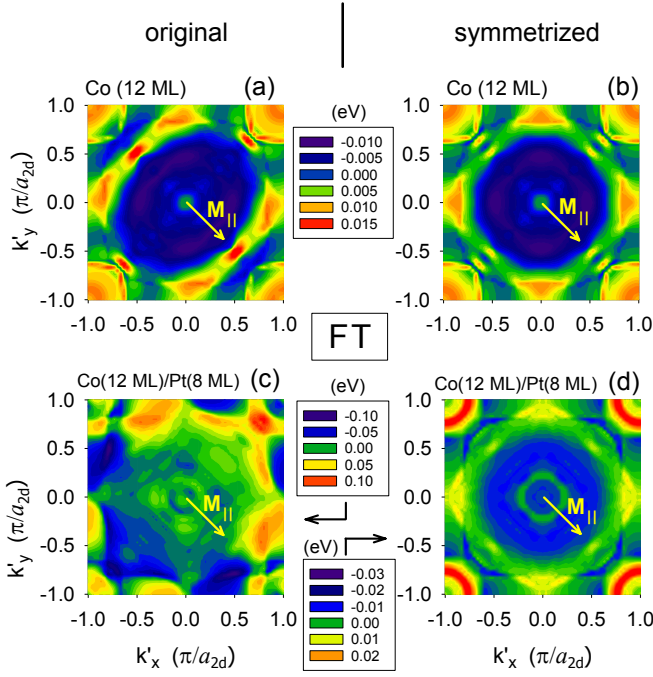


FIG. 26: (a,c) Original and (b,d) symmetrized distributions of the MCA energy in the BZ obtained with the FT for the (001) fcc (a,b) Co(12 ML) film and (c,d) Co(12 ML)/Pt(8 ML) bilayer at $T = 300$ K; see Appendix A. The assumed direction of in-plane magnetization $\mathbf{M}_{||}$ is marked with the yellow arrow. The respective plots for the Co(12 ML) film obtained with the PT are nearly identical within the figure's scale. Note the different scales of the original and symmetrized distributions for the Co(12 ML)/Pt(8 ML) bilayer due to the cancelation of the first-order terms from \mathbf{k} and $-\mathbf{k}$.

the squared matrix elements $|\langle n' \mathbf{k}_i \sigma' | H_{so} | n \mathbf{k}_i \sigma \rangle|^2$ over the different \mathbf{k}_i points. For a general \mathbf{k} point, the wavefunctions $\psi_{n\mathbf{k}_i}^\sigma(\mathbf{r})$ at the points $\mathbf{k}_i = \mathcal{R}_i \mathbf{k}$ are equal to $\psi_{n\mathbf{k}_i}^\sigma(\mathcal{R}_i^{-1} \mathbf{r})$ up to a constant phase factor $e^{i\beta}$. Once the substitution $\mathbf{r}' = \mathcal{R}_i^{-1} \mathbf{r}$ is made, the matrix element $|\langle n' \mathbf{k}_i \sigma' | H_{so} | n \mathbf{k}_i \sigma \rangle|^2$ can

be expressed as $|\langle n' \mathbf{k} \sigma' | H_{so} | n \mathbf{k} \sigma \rangle|^2$ where the spin states are quantized along a rotated magnetization direction. This is either $\mathcal{R}_i \hat{\mathbf{M}}$ or one of other directions $\mathcal{R}_j \hat{\mathbf{M}}$ ($j \neq i$) if the operation \mathcal{R}_i involves only one mirror symmetry ($x \rightarrow -x$ or $y \rightarrow -y$). In either case, the polar angle θ of the magnetization vector \mathbf{M} remains unchanged while its azimuthal angle ϕ is transformed to the respective angle $\phi' = \phi_i$. When the spin quantization axis ζ is oriented along the (θ, ϕ') direction, the matrix element in question may include five distinct angular-dependent terms, proportional to $\sin^2 \theta$, $\sin^2 \theta \cos 2\phi'$, $\sin^2 \theta \sin 2\phi'$, $\sin 2\theta \cos \phi'$ and $\sin 2\theta \sin \phi'$, respectively. The terms originate from the angular dependence of the SOC operator when the spin $\mathbf{S} = (S_x, S_y, S_z)$ is represented in the rotated frame of reference $O\xi\eta\zeta$ [3, 22]. However, upon summing over all eight \mathbf{k}_i points, only the $\sin^2 \theta$ term remains while all other terms, dependent on $\phi' = \phi_i$, completely cancel out. As a result, at any \mathbf{k} point, the symmetrized contribution to the second-order correction $\Omega^{(2)}(\hat{\mathbf{M}})$ to the grand potential depends solely on the polar angle θ (as $\sin^2 \theta$ or, equivalently, as $\cos^2 \theta$), and is independent of the azimuthal angle ϕ . Consequently, the symmetrized distribution of the MCA energy in the BZ defined with Eq. (3) in the PT approach is independent of the choice of the in-plane magnetization direction.

The MCA energy distributions obtained with the FT and PT, both original and symmetrized, are very similar for systems with weak and moderate SOC, like the Co film with the nominal SOC strength; Fig. 26 (a) and (b). For a system without the inversion symmetry, like the Co/Pt bilayer, the original distribution includes finite first-order terms at each \mathbf{k} point. In the PT approach, such terms are excluded from the outset because the total first-order correction $\Omega^{(1)}$ vanishes and the MCA energy is then given by the difference $E_{\text{MCA}}^{\text{PT}} = \Omega^{(2)}(\hat{\mathbf{M}}_{\perp}) - \Omega^{(2)}(\hat{\mathbf{M}}_{||})$. However, these terms persist in the FT calculations. Symmetrization of the MCA energy distribution effectively cancels out these potentially large first-order terms by summing the contributions to $E_{\text{MCA}}^{\text{FT}}$ from the \mathbf{k} and $-\mathbf{k}$ points. In consequence, the resulting symmetrized FT distribution (its leading term) is of the second order. This cancellation effect of the symmetrization is evident in Figs. 26 (c) and (d) (note the different scales in these plots).

-
- [1] J. G. Gay and R. Richter, Phys. Rev. Lett. **56**, 2728 (1986).
 - [2] J. G. Gay and R. Richter, J. Appl. Phys. **61**, 3362 (1987).
 - [3] Chun Li, A. J. Freeman, H. J. F. Jansen, and C. L. Fu Phys. Rev. B **42**, 5433 (1990).
 - [4] P. Bruno, Phys. Rev. B **39**, 865 (1989).
 - [5] M. Cinal, D. M. Edwards, and J. Mathon, Phys. Rev. B **50**, 3754 (1994).
 - [6] M. Dąbrowski, M. Cinal, M. Przybylski, G. Chen, A. T. N'Diaye, A. K. Schmid, and J. Kirschner, Phys. Rev. B **93**, 064414 (2016).
 - [7] M. Dąbrowski, M. Cinal, A. K. Schmid, M. Przybylski, and J. Kirschner, Phys. Rev. B **99**, 184420 (2019).
 - [8] L. Liu, C.-F. Pai, Y. Li, H. W. Tseng, D. C. Ralph, R. A. Buhrman, Science **336**, 555 (2012).
 - [9] L. Liu, O. J. Lee, T. J. Gudmundsen, D. C. Ralph, and R. A. Buhrman, Phys. Rev. Lett. **109**, 096602 (2012).
 - [10] K.-S. Lee, S.-W. Lee, B.-C. Choi, J.-W. Moon, S.-H. Oh, W. Kim, J. Ryu, P. Fischer, and S.-K. Kim, Appl. Phys. Lett. **102**, 112410 (2013).
 - [11] P. D. Bentley, Y. Sasaki, I. Suzuki, S. Isogami, Y. K. Takahashi, and H. Suto, Appl. Phys. Lett. **126**, 022404 (2025).
 - [12] Y.-N. Apriati, K. Nawa, and K. Nakamura, Appl. Phys. Lett. **126**, 082403 (2025).
 - [13] Y. Liu, P. Yang, and P. J. Kelly, Phys. Rev. B **109**, 014416 (2024).
 - [14] W. S. Ham, A.-M. Pradipto, K. Yakushiji, K. Kim, S. H. Rhim, K. Nakamura, Y. Shiota, S. Kim, and T. Ono, npj Computational Materials **7**, 129 (2021).

- [15] A.K. Dhiman, M. Matczak, R. Gieniusz, I. Sveklo, Z. Kurant, U. Guzowska, F. Stobiecki, and A. Maziewski, J. Magn. Mater. **519**, 167485 (2021).
- [16] A.K. Dhiman, A. Fakhredine, R. Gieniusz, Z. Kurant, I. Sveklo, P. Dłużewski, W. Dobrogowski, S. K. Jena, A. Pietruczik, C. Autieri, A. Wawro, A. Maziewski, Appl. Surf. Sci. **679**, 161151 (2025).
- [17] Q. Zhang, J. Liang, K. Bi, L. Zhao, H. Bai, Q. Cui, H.-A. Zhou, H. Bai, H. Feng, et al., Phys. Rev. Lett. **128**, 167202 (2022).
- [18] Q. Liu, L. Liu, G. Xing, and L. Zhu, Nat. Commun. **15**, 2978 (2024).
- [19] M. Weinert, R. E. Watson, and J. W. Davenport, Phys. Rev. B **32**, 2115 (1985).
- [20] X. Wang, D.-S Wang, R. Wu, and A. J. Freeman, J. Magn. Mater. **159**, 337 (1996).
- [21] M. Cinal and D. M. Edwards, Phys. Rev. B **55**, 3636 (1997).
- [22] M. Cinal, Phys. Rev. B **105**, 104403 (2022).
- [23] M. Cinal, Phys. Rev. B **109**, 024424 (2024).
- [24] D.-S Wang, R. Wu, and A. J. Freeman, Phys. Rev. B **47**, 14932 (1993).
- [25] J. Qiao, S. Peng, Y. Zhang, H. Yang, and W. Zhao, Phys. Rev. B **97**, 054420 (2018).
- [26] Y. Miura, S. Ozaki, Y. Kuwahara, M. Tsujikawa, K. Abe, and M. Shirai, J. Phys.: Condens. Matter **25**, 106005 (2013).
- [27] K. Masuda and Y. Miura, Phys. Rev. B **8**, 224421 (2018).
- [28] Y. Miura and J. Okabayashi, J. Phys.: Condens. Matter **34**, 473001 (2022).
- [29] P. V. Ong, N. Kioussis, P. K. Amiri, and K. L. Wang, Phys. Rev. B **94**, 174404 (2016).
- [30] X. Chen, S. Zhang, B. Liu, F. Hu, B. Shen, and J. Sun, Phys. Rev. B **100**, 144413 (2019).
- [31] L. Ke, Phys. Rev. B **99**, 054418 (2019).
- [32] J. Okabayashi, Y. Miura, and H. Muneoka, Sci. Rep. **8**, 8303 (2018).
- [33] D. Li, A. Smogunov, C. Barreteau, F. Ducastelle, and D. Spanjaard, Phys. Rev. B **88**, 214413 (2013).
- [34] D. Li, C. Barreteau, M. R. Castell, F. Silly and A. Smogunov, Phys. Rev. B **90**, 205409 (2014).
- [35] M. Blanco-Rey, J.I. Cerdá and A. Arnau, New J. Phys. **21**, 073054 (2019).
- [36] L. Szunyogh, B. Újfalussy, C. Blaas, U. Pustogowa, C. Sommers, and P. Weinberger Phys. Rev. B **56**, 14036 (1997).
- [37] G. Y. Guo, J. Phys.: Condens. Matter **11**, 4329 (1999).
- [38] M. Cinal, J. Phys.: Condens. Matter **15**, 29 (2003).
- [39] L. M. Sandratskii, Phys. Rev. B **92**, 134414 (2015).
- [40] S. Manna, P. L. Gastelois, M. Dąbrowski, P. Kuświk, M. Cinal, M. Przybylski, and J. Kirschner, Phys. Rev. B **87**, 134401 (2013).
- [41] M. Cinal and D.M. Edwards, Phys. Rev. B **57**, 100 (1998).
- [42] M. Cinal, J. Phys.: Condens. Matter **13**, 901 (2001).
- [43] C.-H. Chang, K.-P. Dou, G.-Y. Guo, and C.-C. Kaun, NPG Asia Materials **9**, e424 (2017).
- [44] J. Marciniak, M. Werwiński, J. Magn. Mater. **609**, 172455 (2024).
- [45] D. M. Edwards, J. Mathon, R. B. Muniz, and M. S. Phan, Phys. Rev. Lett. **67**, 493 (1991); Erratum Phys. Rev. Lett. **67**, 1476 (1991).
- [46] U. Bauer, M. Dąbrowski, M. Przybylski, and J. Kirschner, Phys. Rev. B **84**, 144433 (2011).
- [47] M. Przybylski, M. Dąbrowski, U. Bauer, M. Cinal, and J. Kirschner, J. Appl. Phys. **111**, 07C102 (2012).
- [48] S. Manna, M. Przybylski, D. Sander, J. Kirschner, J. Phys. Condens. Matter **28**, 456001 (2016).
- [49] J. Li, M. Przybylski, F. Yildiz, X. D. Ma, and Y. Z. Wu, Phys. Rev. Lett. **102**, 207206 (2009).
- [50] M. Ślęzak, P. Drózd, K. Matlak, A. Koziół-Rachwał, J. Korecki, and T. Ślęzak, J. Magn. Mater. **497**, 165963 (2020).
- [51] T.H. Moos, W. Hübner, K.H. Bennemann, Solid State Comm. **98**, 639 (1996).
- [52] A. Lessard, T. H. Moos, and W. Hübner, Phys. Rev. B **56**, 2594 (1997).
- [53] T. Balcerzak, Thin Solid Films **500**, 341 (2006).
- [54] E. Abate and M. Asdente, Phys. Rev. **140**, A1303 (1965).
- [55] D.A. Papaconstantopoulos, *Handbook of the Band Structure of Elemental Solids* (Plenum, New York, 1986).
- [56] C. S. Wang and A. J. Freeman, Phys. Rev. B **19**, 793 (1979).
- [57] O. Jepsen and O. K. Andersen, Solid State Commun. **9**, 1763 (1971).
- [58] E. Barati, M. Cinal, D. M. Edwards, and A. Umerski, Phys. Rev. B **90**, 014420 (2014).
- [59] E. Barati and M. Cinal, Phys. Rev. B **91**, 214435 (2015).
- [60] J. M. Soler, E. Artacho, J. D. Gale, A. García, J. Junquera, P. Ordejón, and D. Sánchez-Portal, J. Phys.: Condens. Matter **14**, 2745 (2002).
- [61] G. Kresse and J. Hafner, Phys. Rev. B **47**, 558 (1993); *ibid.* **49**, 14 251 (1994)]
- [62] G. Kresse and J. Furthmüller, Phys. Rev. B **54**, 11169 (1996).